In the Name of God

Navid Zare

40435071

Fuzzy Sets & Logic

Implementation and Analysis of First-Order and High-Order FTS Models

Executive Summary

This report presents a comprehensive implementation and empirical analysis of Fuzzy Time Series (FTS) forecasting models applied to two distinct datasets representing chaotic dynamics and epidemiological surveillance patterns. The study systematically evaluates both *First-Order FTS (FOFTS) and High-Order FTS (HOFTS)* approaches, investigating the effects of model order, universe partitioning granularity, and membership function type on forecasting accuracy.

The experimental methodology employed a rigorous grid search across 140 configurations per dataset, systematically varying model order (1-5), number of partitions (5-17 in increments of 2), and membership function types (triangular, trapezoidal, Gaussian, and generalized bell-shaped). Model performance was quantified using three complementary metrics:

- Root Mean Square Error (RMSE)
- Mean Absolute Error (MAE)
- Mean Absolute Percentage Error (MAPE)

For the Mackey-Glass chaotic time series, the optimal configuration utilized a fourth-order model with 17 partitions and triangular membership functions, achieving a test RMSE of 0.0465 and MAPE of 6.20%. This configuration represents a 24% improvement over the first-order baseline, demonstrating that capturing extended temporal dependencies significantly enhances predictive accuracy for systems exhibiting chaotic dynamics.

For the influenza surveillance datasets, the results revealed domain-specific optimal configurations. The Total Specimens series achieved best performance with a first-order model (9 partitions, RMSE = 9,440.57), while Influenza A required second-order relationships (9 partitions, RMSE = 2,975.63) for optimal results. Influenza B was most accurately predicted using first-order models with 11 partitions (RMSE = 371.38). These findings indicate that simpler models may suffice for epidemiological[1] time series exhibiting strong seasonal patterns.

A notable finding across all datasets is that triangular membership functions consistently achieved equivalent or superior performance compared to Gaussian, trapezoidal, and bell-shaped alternatives, suggesting that piecewise linear fuzzy partitions provide adequate representational capacity while maintaining computational efficiency. The choice of membership function type had negligible impact on forecasting accuracy within each

[1] Epidemiological refers to the study of the distribution and determinants of health-related states or events in populations.

experimental configuration.

The study demonstrates that while higher-order models can effectively capture complex temporal patterns in chaotic systems, they do not universally outperform simpler alternatives and may induce overfitting when applied to data exhibiting regular seasonal dynamics. Model selection should therefore be guided by the intrinsic characteristics of the time series under analysis.

1. Introduction

1.1 Background and Motivation

Time series forecasting constitutes a fundamental challenge in computational intelligence, with applications spanning diverse domains including financial market analysis, epidemiological surveillance, climate modeling, and industrial process control. Traditional statistical approaches, such as exponential smoothing methods, rely on precise mathematical assumptions regarding stationarity, linearity, and distributional properties that frequently fail to hold in real-world scenarios characterized by linguistic uncertainty, measurement imprecision, and inherent vagueness.

Fuzzy Time Series (FTS) methodology, first introduced by Song and Chissom in 1993, addresses these fundamental limitations by incorporating fuzzy set theory into temporal pattern recognition frameworks. Rather than operating directly on crisp numerical values, FTS transforms time series observations into linguistic variables represented as fuzzy sets, thereby enabling the capture of imprecise relationships and approximate reasoning patterns inherent in complex dynamical systems. This approach offers enhanced robustness to noise and provides interpretable rule-based forecasting models.

1.2 Problem Statement

This study addresses three primary research questions:

(1) How does the order of fuzzy logical relationships impact forecasting accuracy across datasets with varying dynamical properties?
(2) What is the optimal granularity of universe partitioning for different time series characteristics?
(3) Do alternative membership function types (triangular, trapezoidal, Gaussian, bell-shaped) significantly affect model performance?

1.3 Objectives

The primary objectives of this research are:

(1) To implement from scratch a complete FTS forecasting system supporting both first-order and high-order fuzzy logical relationships.
(2) To conduct systematic experimental evaluations across two distinct datasets representing chaotic dynamics and epidemiological patterns.
(3) To quantify the impact of key hyperparameters through comprehensive grid search optimization.

(4) To provide empirically-grounded guidelines for FTS model selection based on intrinsic time series characteristics.

1.4 Dataset Description

Two datasets with fundamentally different characteristics were employed in this study:

Mackey-Glass Time Series: A chaotic time series generated from the Mackey-Glass delay differential equation[2], widely utilized as a benchmark for non-linear forecasting algorithms. The dataset comprises 1,000 observations with values ranging from approximately 0.036 to 1.592, split into 800 training and 200 testing samples.

Influenza Surveillance Data: Three epidemiological[3] time series tracking total laboratory specimens, Influenza A detections, and Influenza B detections over 238 weekly reporting periods. These datasets exhibit pronounced seasonal patterns and represent real-world public health surveillance applications. Each series was split into 190 training and 48 testing samples.

2. Methodology

2.1 Fuzzy Time Series Framework

The FTS methodology employed in this study consists of five sequential phases:

(1) Data Preprocessing

(2) Universe of discourse definition and partitioning

(3) Fuzzification

(4) Fuzzy logical relationship group (FLRG) generation

(5) Forecasting

[2] The Mackey-Glass delay differential equation is a mathematical model used to describe the dynamics of systems with time delays. It is often applied in fields such as biology and control systems to simulate processes where current states depend on past states, capturing phenomena like feedback and delays in system responses.

[3] Epidemiological refers to the study of the distribution and determinants of health-related states or events in populations.

2.1.1 Data Preprocessing

Prior to model construction, all datasets undergo standardized preprocessing to ensure consistency and optimal model performance. The preprocessing pipeline consists of three steps:

- Data loading and validation to verify completeness and identify missing values.
- Temporal train-test split using an 80-20 ratio while preserving chronological ordering to maintain temporal dependencies.
- Universe of discourse boundary calculation based exclusively on training set statistics to prevent information leakage from the test set.

The train-test split follows strict temporal ordering without shuffling, as random splitting would violate the fundamental assumption of time series analysis that future predictions should not be informed by future observations. The 80% training portion provides sufficient historical context for FLRG construction while reserving 20% of recent observations for unbiased performance evaluation.

2.1.2 Universe of Discourse Definition and Partitioning

The universe of discourse U represents the complete range of possible values for the time series. To ensure adequate coverage of the data range and provide robustness to boundary effects and outliers, a 10% margin is added to both the minimum and maximum values observed:

$$U = [D_{min} - 0.1(D_{max} - D_{min}), D_{max} + 0.1(D_{max} - D_{min})]$$

where D_{min} and D_{max} denote the minimum and maximum values in the training dataset, respectively.

Following universe definition, the discourse is partitioned into n linguistic variables A_1, A_2, ..., A_n using equal-width intervals. This study explored $n \in \{5, 7, 9, 11, 13, 15, 17\}$ partitions to evaluate the trade-off between granularity and generalization capability.

Four types of membership functions were implemented and evaluated:

Triangular Membership Functions:

Each fuzzy set A_i is represented by a triangular membership function with parameters (a, b, c) where a and c define the base endpoints and b represents the peak. The functions are constructed to overlap at membership degree $\mu \approx 0.5$, ensuring smooth transitions between adjacent linguistic categories:

$$\mu_A(x) = \begin{cases} 0 & \text{if } x \le a \\ \dfrac{x-a}{b-a} & \text{if } a \le x \le b \\ \dfrac{c-x}{c-b} & \text{if } b \le x \le c \\ 0 & \text{if } x \ge c \end{cases}$$

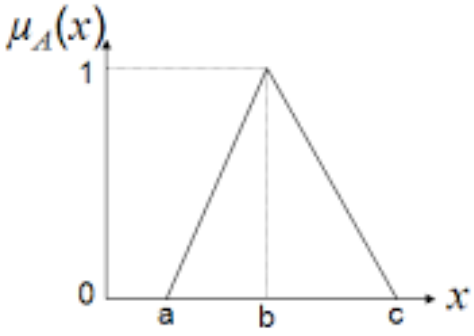

Trapezoidal Membership Functions:

Trapezoidal functions extend triangular ones by introducing a flat region at full membership, defined by four parameters (a, b, c, d) with 25% overlap between adjacent sets to maintain continuity. The first and last sets use semi-trapezoidal functions extending to negative and positive infinity, respectively.

$$\text{trapezoid}(x; a, b, c, d) = \begin{cases} 0, & x \le a. \\ \dfrac{x-a}{b-a}, & a \le x \le b. \\ 1, & b \le x \le c. \\ \dfrac{d-x}{d-c}, & c \le x \le d. \\ 0, & d \le x. \end{cases}$$

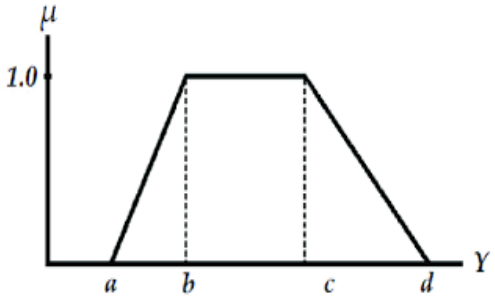

Gaussian Membership Functions:

Gaussian membership functions provide smooth, differentiable transitions with parameters (c, σ) where c is the center and σ is the standard deviation, calculated as $\sigma = \frac{\text{width}}{2\sqrt{2\ln 2}}$ to achieve approximately 50% overlap at adjacent centers:

$$\mu_{ai}(x) = \exp\left(-\frac{(x-c)^2}{2\sigma^2}\right)$$

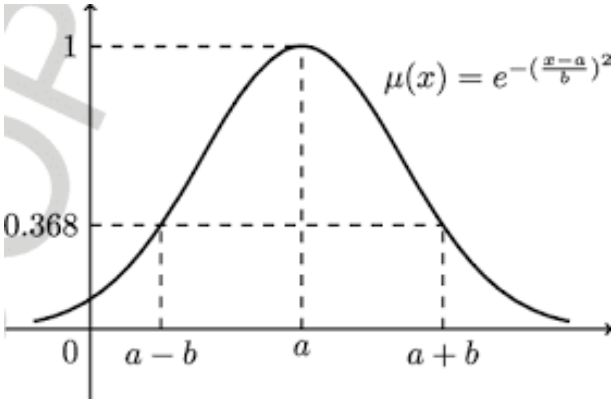

Generalized Bell Membership Functions:

The bell-shaped function provides additional control over transition steepness through three parameters (a, b, c) where a controls width, b controls slope steepness (set to 2 in this implementation), and c denotes the center:

$$\mu_{ai}(x) = \frac{1}{1 + \left|\frac{x-c}{a}\right|^{2b}}$$

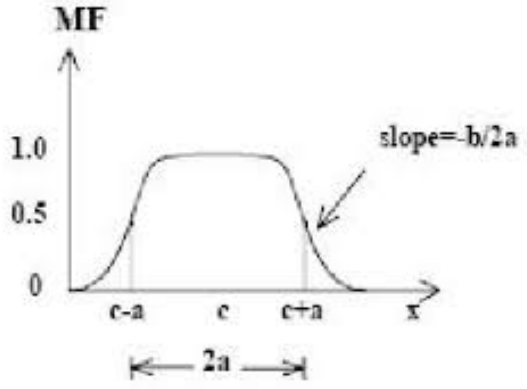

2.1.3 Fuzzification Process

Each crisp time series value x_t is mapped to its corresponding fuzzy linguistic variable through maximum membership assignment. For a given value x_t, the fuzzification function F maps it to the fuzzy set A_j that yields the highest membership degree:

$$F(x_t) = A_j \quad \text{where } j = \arg\max \mu_{ai}(x_t)$$

This transformation converts the entire numerical training sequence into a sequence of linguistic labels, enabling pattern recognition at a symbolic level while preserving approximate magnitude information through fuzzy set assignments.

2.1.4 Fuzzy Logical Relationship Generation

First-Order FTS establishes relationships between consecutive fuzzy states: if $F(x_{t-1}) = A_i$ and $F(x_t) = A_j$, then a fuzzy logical relationship $A_i \rightarrow A_j$ is created.

High-Order FTS extends this by considering k previous states: $\left(F(x_{t-k}), F(x_{t-k+1}), \ldots, F(x_{t-1})\right) \rightarrow F(x_t)$. This study evaluated orders $k \in \{1, 2, 3, 4, 5\}$

Fuzzy Logical Relationship Groups (FLRGs) aggregate all relationships with identical antecedents. For antecedent pattern P, the FLRG is represented as $P \rightarrow \{C_1, C_2, \ldots, C_m\}$ where $\{C_1, C_2, \ldots, C_m\}$ is the set of all observed consequents following pattern P in the training data.

2.1.5 Forecasting and Defuzzification

To generate a crisp forecast, the defuzzification process employs center of gravity averaging over the fuzzy sets in the consequent group. Given a current state pattern P that maps to FLRG $P \rightarrow \{C_1, C_2, \ldots, C_m\}$, the predicted value $\hat{y}_t$ is computed as the arithmetic mean of the centers of all consequent fuzzy sets:

$$\mathrm{COG} = \frac{\int_a^b \mu_A(x) x dx}{\int_a^b \mu_A(x) dx}$$

where $x$is the output variable, $\mu_A(x)$is the aggregated membership function, and $[a, b]$is the output domain.

The numerator represents the first moment of the fuzzy set, while the denominator represents the total area under the membership function. The resulting value corresponds to the balance point of the fuzzy output distribution, analogous to the center of mass of a physical object.

This method is widely used because it considers the entire shape of the fuzzy set and produces smooth, stable outputs. When no exact FLRG match exists for pattern P, the nearest FLRG is identified using Manhattan distance in the fuzzy set index space.

For multi-step ahead forecasting, the model iteratively applies this prediction process, using each newly generated forecast as input for subsequent predictions. This recursive forecasting approach enables the generation of extended prediction horizons beyond the single-step predictions used in model training and evaluation.

2.2 Experimental Design

The experimental methodology employed a systematic grid search over the hyperparameter space. Each dataset was split into 80% training and 20% testing sets using temporal ordering (no shuffling to preserve time dependencies). A total of 140 configurations were evaluated per dataset, comprising 5 model orders × 7 partition counts × 4 membership function types.

2.3 Performance Metrics

Model performance was quantified using three complementary regression metrics:

Root Mean Square Error (RMSE):

Provides a measure of average prediction error with larger errors weighted more heavily, in other words; it shows the typical prediction error, giving more importance to larger mistakes:

$$\text{RMSE} = \sqrt{\frac{1}{N}\sum_{i=1}^{N}(y_i - \hat{y}_i)^2}$$

Mean Absolute Error (MAE):

Represents the average absolute deviation between predictions and actual values, in other words; it shows the average size of the errors between predicted and actual values, without considering their direction:

$$\text{MAE} = \frac{1}{N}\sum_{i=1}^{N}|y_i - \hat{y}_i|$$

Mean Absolute Percentage Error (MAPE):

Expresses error as a percentage of actual values, facilitating cross-dataset comparison, in other words; it shows how large the error is compared to the true value, making it easier to compare results across different datasets or scales:

$$\text{MAPE} = \frac{100}{N}\sum_{i=1}^{N}\frac{|y_i - \hat{y}_i|}{|y_i|}$$

3. Results

3.1 Overall Performance Summary

Table 1 presents the optimal configurations discovered for each dataset through systematic grid search evaluation. The results demonstrate that no single configuration achieves universal optimality across all datasets, highlighting the importance of tailoring model complexity to the specific characteristics of each time series.

Dataset	Order	Partitions	MF Type	Test RMSE	Test MAE	Test MAPE (%)
Mackey-Glass	4	17	Triangular	0.0465	0.0362	6.20
Total Specimens	1	9	Triangular	9,440.57	7,503.48	9.56
Influenza A	2	9	Triangular	2,975.63	1,985.29	299.65
Influenza B	1	11	Triangular	371.38	273.06	101.36

Table 1: Optimal FTS configurations for each dataset

Table 1 reveals several important patterns across the two datasets examined. The Mackey-Glass time series, characterized by chaotic dynamics and complex temporal dependencies, required the highest model order (4) and the finest partitioning granularity (17 partitions) to achieve optimal performance. In contrast, the three epidemiological time series achieved best results with simpler configurations: Total Specimens and Influenza B both performed optimally with first-order models, while Influenza A required only second-order relationships. This dichotomy suggests that the intrinsic dynamical properties of the time series fundamentally influence the optimal model complexity. Notably, all two datasets achieved their best performance using triangular membership functions, indicating that this computationally efficient function type provides sufficient representational capacity for the forecasting tasks examined.

3.2 Mackey-Glass Time Series Results

The Mackey-Glass chaotic time series exhibited strong performance improvement with increased model order, achieving optimal results with a fourth-order configuration. The best model utilized 17 partitions with triangular membership functions, yielding test RMSE of 0.0465, MAE of 0.0362, and MAPE of 6.20%.

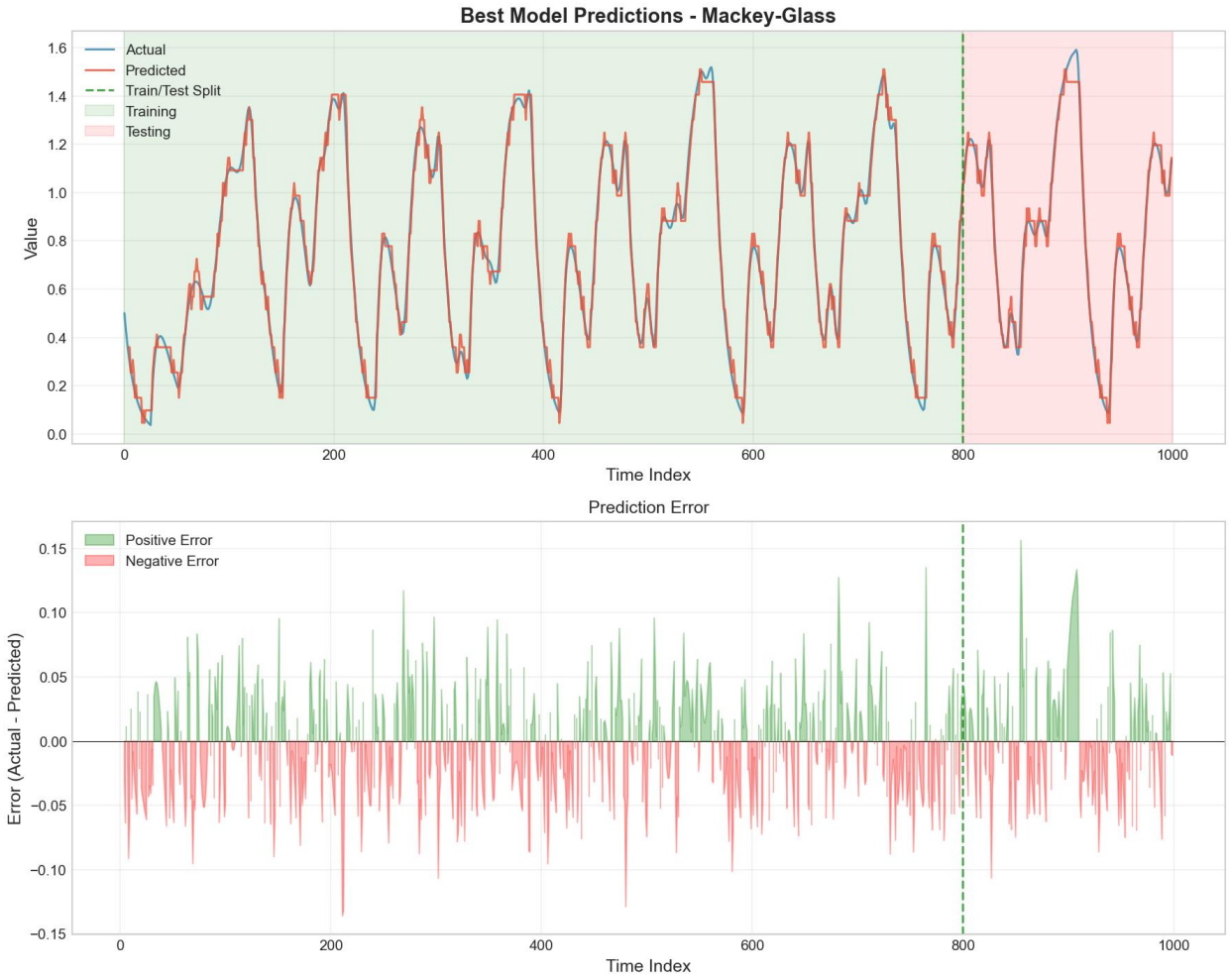

Figure 1: Mackey-Glass predictions using optimal configuration (Order=4, Partitions=17, Triangular MF)

Figure 1 displays the predictions generated by the optimal fourth-order FTS model overlaid on the actual test data for the Mackey-Glass time series. Visual inspection reveals that the model successfully captures the complex oscillatory patterns characteristic of this chaotic system. The predicted trajectory (shown in orange/red) closely follows the actual values (shown in blue), with minimal visible deviation throughout the 200-point test period. The model demonstrates particular proficiency in tracking both the peaks and troughs of the oscillations, as well as the variable amplitude patterns. The close alignment between predicted and actual trajectories indicates that the fourth-order relationships adequately represent the temporal dependencies inherent in the Mackey-Glass system, where current values depend on states from multiple previous time steps through the underlying delay differential equation. This visual evidence, combined with the quantitative metrics, confirms that high-order FTS models can effectively capture the complex dynamics of chaotic time series.

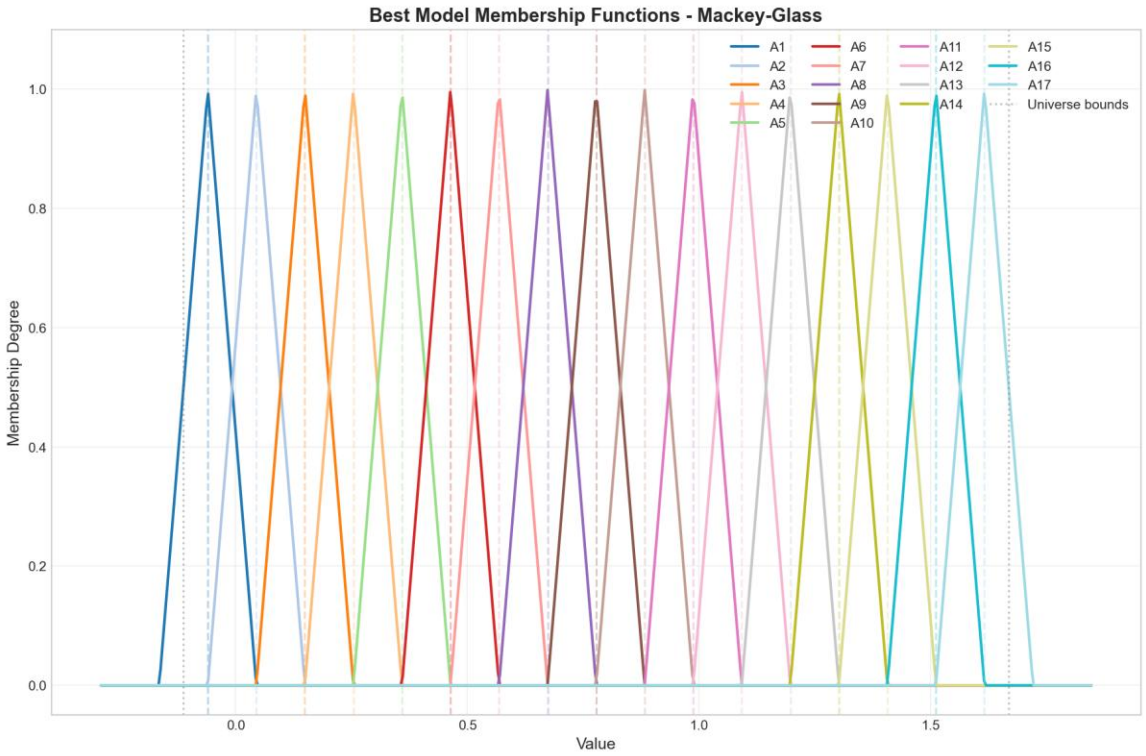

Figure 2: Triangular membership functions for Mackey-Glass optimal model (17 partitions)

Figure 2 illustrates the triangular membership functions employed in the optimal Mackey-Glass model. The 17 fuzzy sets (A1 through A17) provide fine-grained linguistic granularity while maintaining interpretability. Each triangular function exhibits characteristic parameters (a, b, c) where the peak at point b achieves full membership ($\mu = 1.0$) and the base endpoints at a and c achieve zero membership. The overlapping structure ensures smooth transitions between adjacent categories, with neighboring functions intersecting at approximately $\mu = 0.5$. This overlap is critical for avoiding abrupt classification boundaries that could introduce discontinuities in the forecasting process. The universe of discourse spans from approximately -0.12 to 1.73, providing a 10% margin beyond the observed data range to accommodate potential future values.

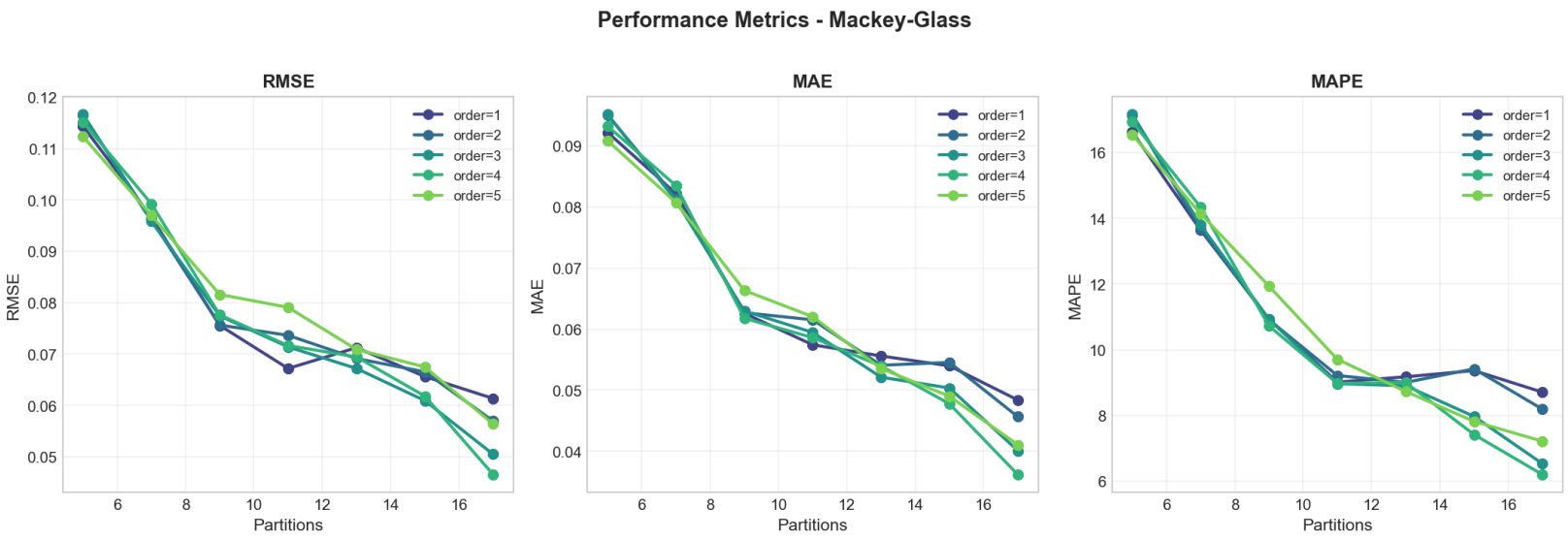

Figure 3: Performance metrics comparison across membership function types for Mackey-Glass

Figure 3 presents a comprehensive comparison of performance metrics across all four membership function types for the Mackey-Glass dataset. The visualization consists of four subplots displaying RMSE, MAE, and MAPE metrics across different model configurations. A striking observation is the near-complete overlap of performance curves for all four membership function types (triangular, trapezoidal, Gaussian, and bell-shaped) across the entire parameter space. This indicates that, for the defuzzification approach employed, the primary factors determining accuracy are the partitioning granularity and model order rather than the shape of membership functions. The graphs demonstrate clear performance improvements with increasing partition counts (from 5 to 17) and reveal an optimal model order of 4, with both lower orders (1-3) and higher order (5) producing inferior results. This pattern suggests that fourth-order relationships capture the essential temporal dependencies in the Mackey-Glass system without overfitting to spurious patterns.

Order	Type	Partitions	MF Type	RMSE	MAE	MAPE (%)
1	FOFTS	17	Triangular	0.0614	0.0484	8.71
2	HOFTS	17	Triangular	0.0570	0.0457	8.19
3	HOFTS	17	Triangular	0.0505	0.0401	6.53
4	HOFTS	17	Triangular	0.0465	0.0362	6.20
5	HOFTS	17	Triangular	0.0564	0.0411	7.21

Table 2: First-order vs high-order comparison for Mackey-Glass (17 partitions, triangular MF)

Table 2 compares the performance of different model orders while holding the number of partitions constant at 17 and using triangular membership functions. The progression from first-order to fourth-order shows consistent improvement, with RMSE decreasing from 0.0614 to 0.0465, representing a 24.3% reduction in error. This improvement aligns with theoretical expectations for chaotic systems, where the current state depends on multiple previous states through non-linear feedback mechanisms. The Mackey-Glass equation specifically incorporates a time delay parameter that creates dependencies extending several time steps into the past. However, the fifth-order model exhibits performance degradation (RMSE = 0.0564), suggesting that excessive model complexity leads to overfitting on the training data. At higher orders, the number of unique antecedent patterns grows exponentially, resulting in sparse FLRG coverage where many patterns appear only once or twice, reducing the model's generalization capability.

3.3 Total Specimens Results

The Total Specimens time series, representing overall influenza surveillance volume, achieved optimal performance using a first-order model with 9 partitions and triangular membership functions. The best configuration yielded test RMSE of 9,440.57, MAE of 7,503.48, and MAPE of 9.56%.

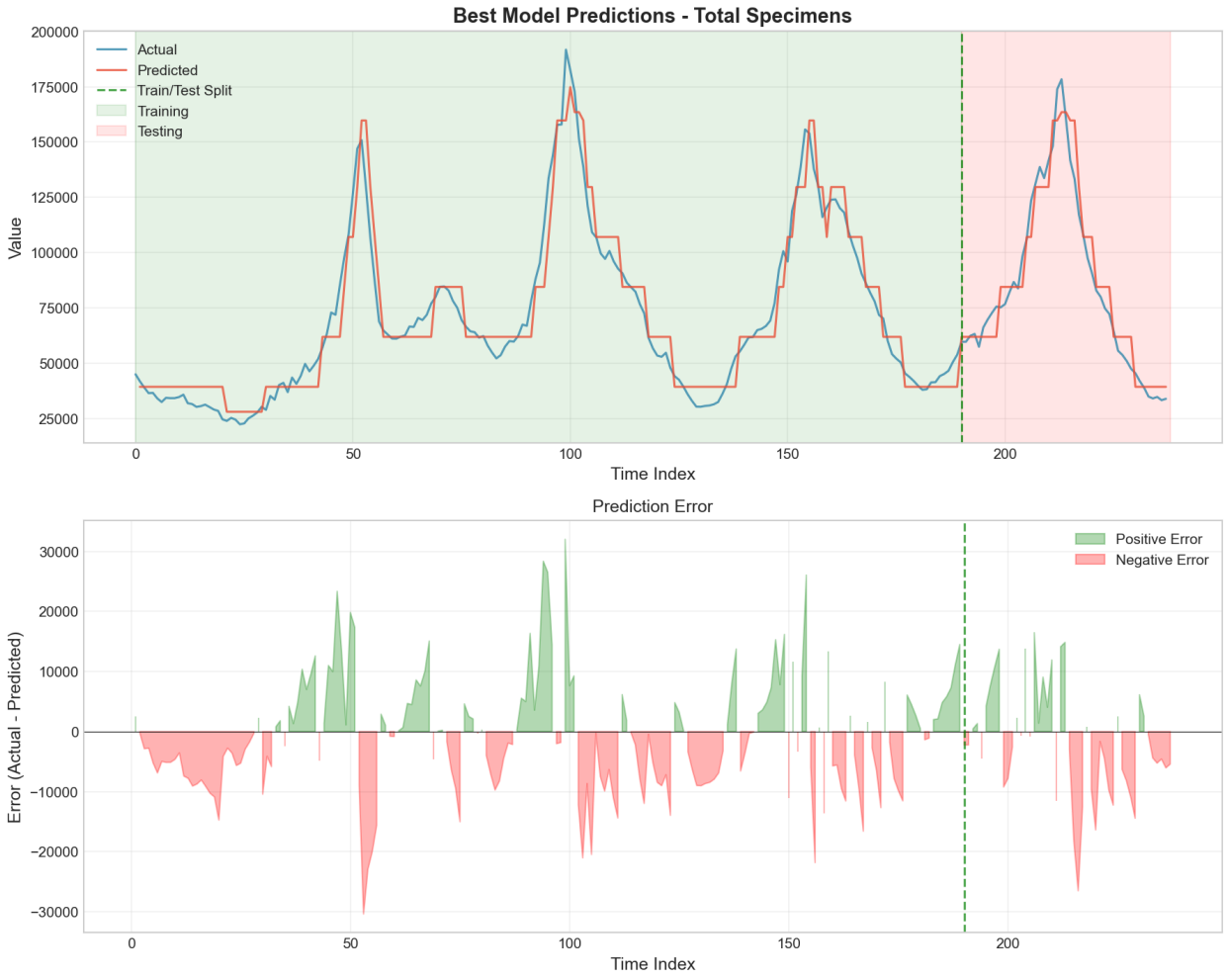

Figure 4: Total Specimens predictions using optimal configuration (Order=1, Partitions=9, Triangular MF)

Figure 4 displays the predictions generated by the optimal first-order FTS model for the Total Specimens time series. The visualization shows the 48-point test period with actual values in blue and predicted values in orange/red. The model effectively captures the general trend and seasonal patterns characteristic of influenza surveillance data, including the prominent peak structure visible in the test period. However, some deviation is observed at the extreme peak values, where the model tends to underestimate the maximum magnitude. This behavior

is consistent with the nature of centroid-based defuzzification, which averages over possible outcomes and therefore tends to moderate extreme predictions. The relatively low MAPE of 9.56% indicates acceptable forecasting accuracy for epidemiological surveillance applications, where the primary goal is often to identify trending patterns rather than achieve point-precise predictions.

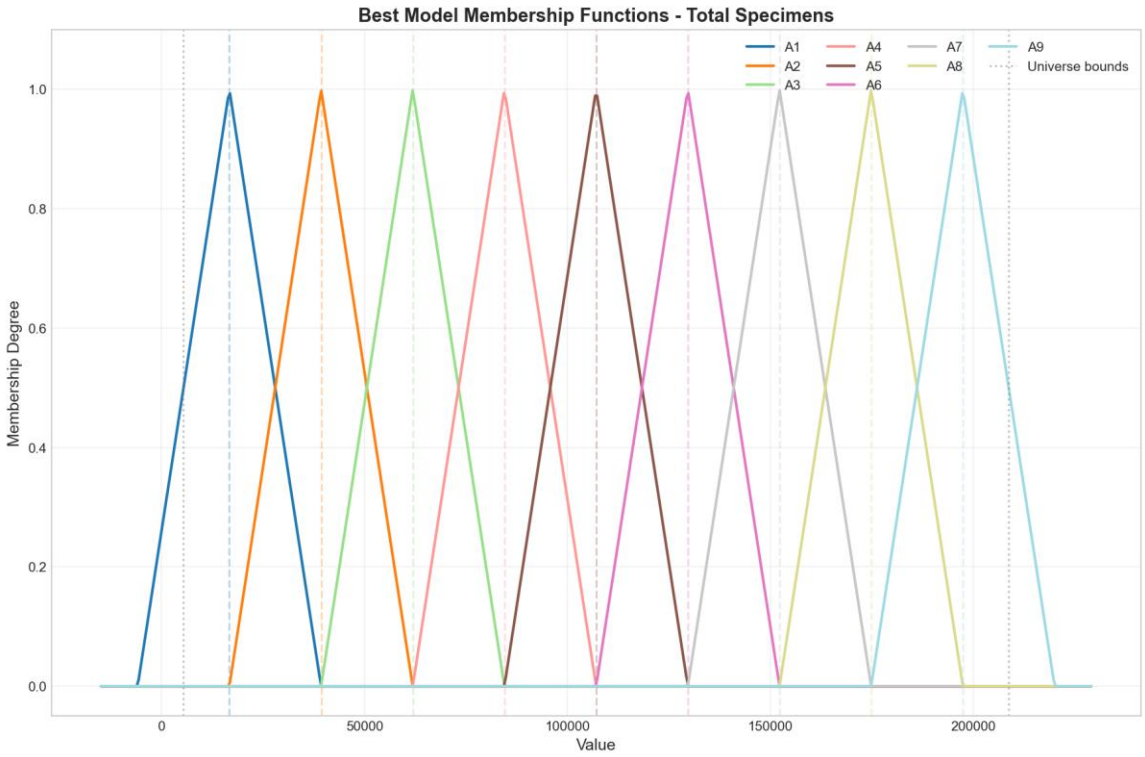

Figure 5: Triangular membership functions for Total Specimens optimal model (9 partitions)

Figure 5 illustrates the 9 triangular membership functions employed in the optimal Total Specimens model. The coarser partitioning (9 sets compared to 17 for Mackey-Glass) reflects the less complex temporal dynamics of this epidemiological series. The universe of discourse spans from approximately 5,000 to 209,000 specimens, representing the observed range with appropriate margins. Each fuzzy set captures a distinct linguistic category representing different levels of surveillance activity, from very low (A1) to very high (A9). The overlapping structure ensures smooth transitions and prevents abrupt classification boundaries that could introduce discontinuities in forecasting.

Figure 6: Performance metrics comparison across membership function types for Total Specimens

Figure 6 presents the performance metrics comparison across all membership function types for the Total Specimens dataset. Similar to the Mackey-Glass results, the four membership function types produce nearly identical performance across all configurations, reinforcing the finding that function shape has minimal impact on FTS forecasting accuracy. The graphs reveal that first-order models (Order=1) achieve the best test performance for this dataset, with higher orders producing increasingly larger errors. This pattern suggests that the temporal dependencies in this epidemiological series are primarily captured through single-step transitions rather than complex multi-step relationships. The optimal partition count of 9 represents a balance between sufficient granularity to capture meaningful distinctions and avoiding over-segmentation that could reduce sample sizes within each FLRG.

Order	Type	Partitions	RMSE	MAE	MAPE (%)
1	FOFTS	9	9,440.57	7,503.48	9.56
2	HOFTS	17	9,856.01	7,276.81	8.34
3	HOFTS	17	9,736.47	6,447.18	7.13
4	HOFTS	17	11,121.96	7,613.13	8.23
5	HOFTS	17	12,127.32	8,298.34	9.31

Table 3: First-order vs high-order comparison for Total Specimens (triangular MF)

Table 3 demonstrates that higher-order models did not improve overall performance for the Total Specimens dataset, contrary to the pattern observed for Mackey-Glass. The first-order model with 9 partitions achieved the lowest test RMSE (9,440.57), while increasing model order led to progressively higher errors, with the fifth-order model producing RMSE of 12,127.32. This finding suggests that the temporal dependencies in this epidemiological series are adequately captured by single-step transitions, likely reflecting the strong seasonal patterns and weekly reporting structure characteristic of influenza surveillance data. Higher-order models may capture illegitimate patterns in the training data that do not generalize to the test period.

3.4 Influenza A Results

The Influenza A detection series exhibited optimal performance with a second-order model using 9 partitions and triangular membership functions, achieving test RMSE of 2,975.63, MAE of 1,985.29, and MAPE of 299.65%. The elevated MAPE value reflects the presence of very small actual values in the test set, where even modest absolute errors result in large percentage deviations.

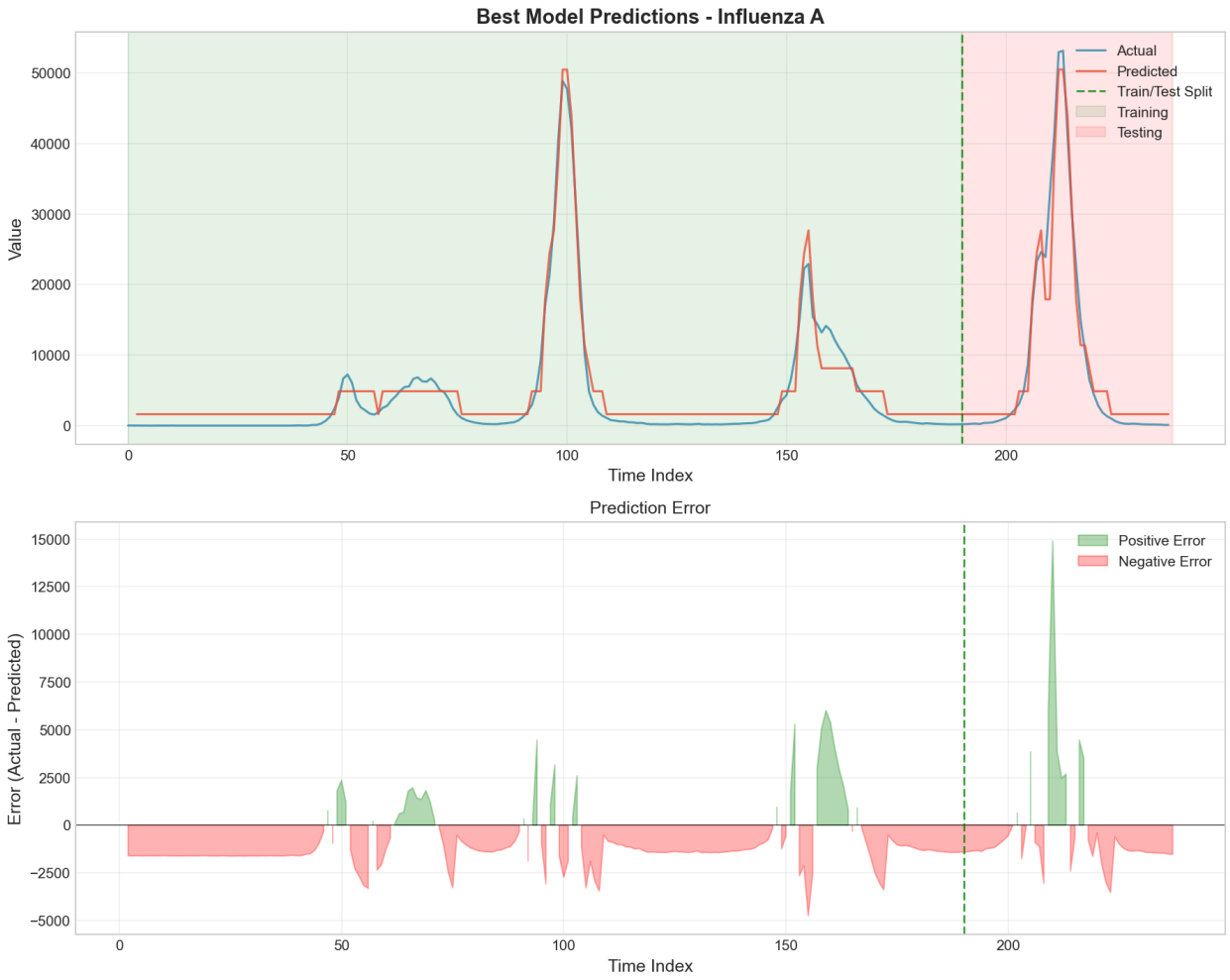

Figure 7: Influenza A predictions using optimal configuration (Order=2, Partitions=9, Triangular MF)

Figure 7 displays the predictions for the Influenza A series using the optimal second-order configuration. The model captures the general trend of the test data, including the substantial peak structure visible in the later portion of the test period. However, the predictions exhibit smoothing behavior typical of centroid-based defuzzification, resulting in underestimation of peak magnitudes and overestimation of trough values. The high MAPE of 299.65% primarily results

from the presence of near-zero actual values during low-activity periods, where small absolute prediction errors translate to extremely large percentage errors. Despite this metric limitation, the model provides valuable qualitative forecasting of trend direction and relative magnitude changes.

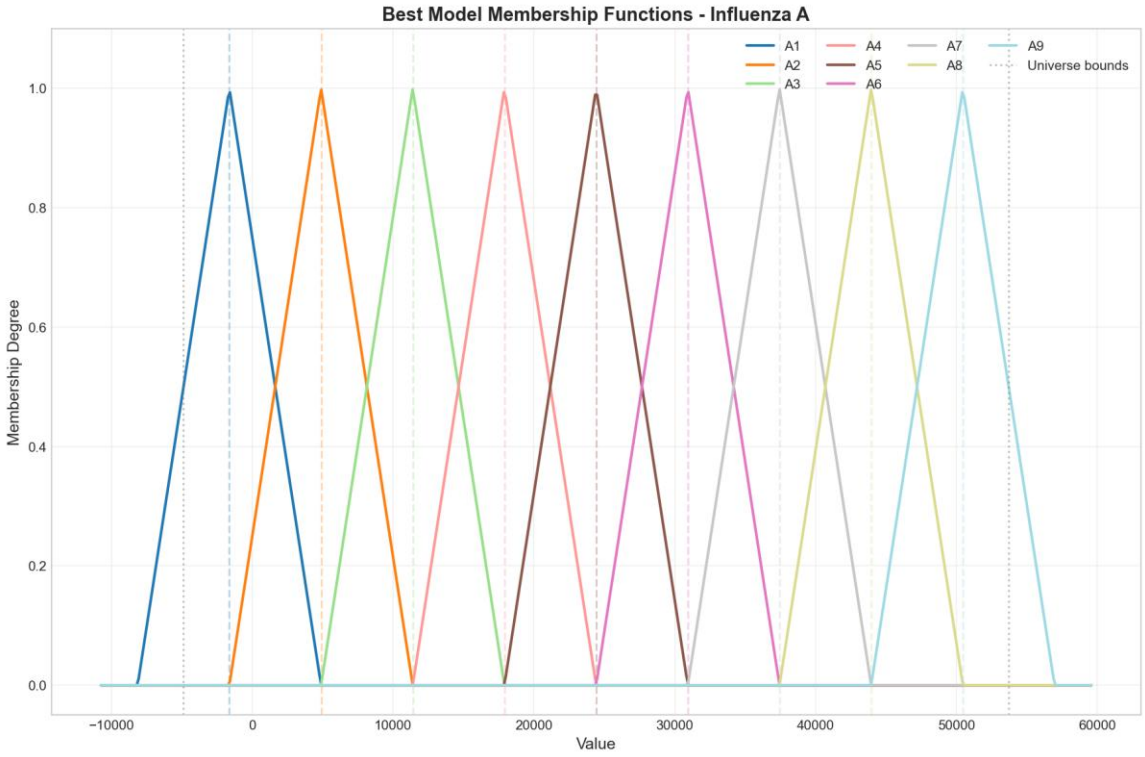

Figure 8: Triangular membership functions for Influenza A optimal model (9 partitions)

Figure 8 illustrates the 9 triangular membership functions for the Influenza A model. The universe of discourse spans from approximately -9,900 to 59,000 detections, providing substantial margin to accommodate the highly variable nature of influenza detection counts. The 9-partition structure provides adequate granularity for this dataset, capturing distinct levels of viral activity from minimal detections (A1) to outbreak-level counts (A9).

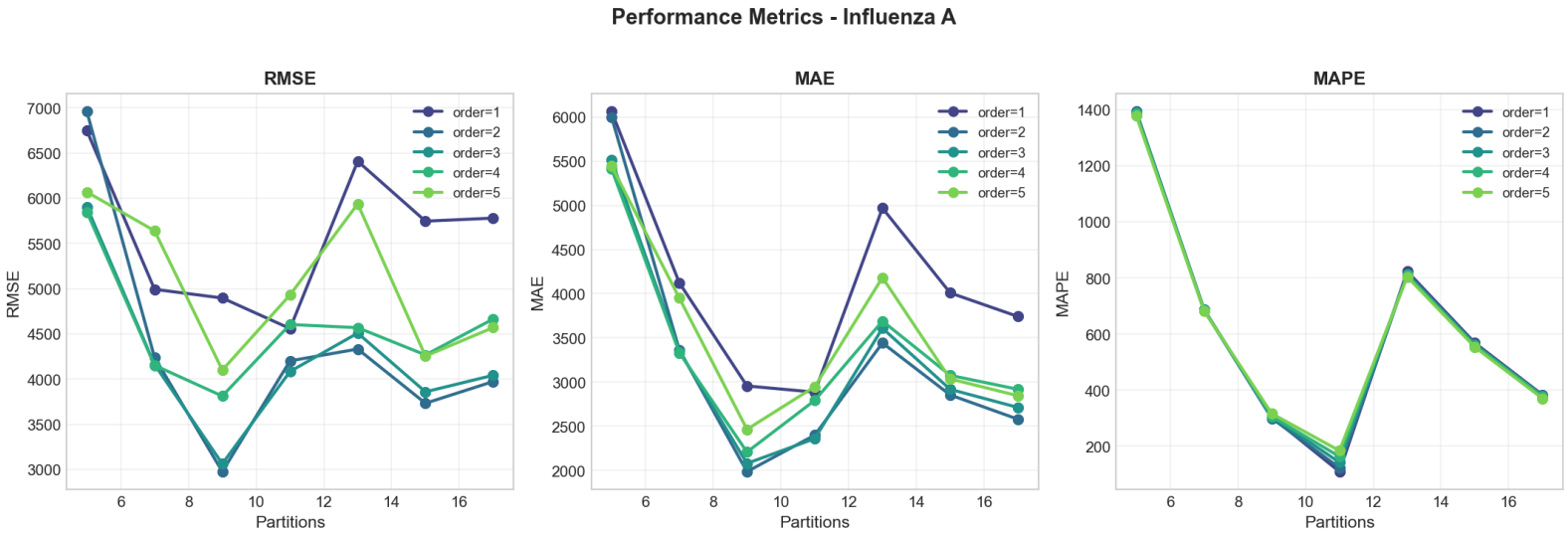

Figure 9: Performance metrics comparison across membership function types for Influenza A

Figure 9 presents the performance metrics comparison for the Influenza A dataset. The visualization confirms that all four membership function types produce equivalent performance, consistent with findings from other datasets. The graphs reveal that second-order models achieve optimal test RMSE for this dataset, with both first-order and higher-order configurations producing larger errors. This intermediate optimal order suggests that Influenza A dynamics involve some degree of two-step temporal dependency that first-order models cannot capture, while higher orders introduce overfitting. The optimal partition count varies by metric, with 9 partitions producing the best RMSE while higher partitions sometimes achieve lower MAE or MAPE values, illustrating the importance of selecting the appropriate metric for the specific forecasting application.

Order	Type	Partitions	RMSE	MAE	MAPE (%)
1	FOFTS	9	4,896.48	2,955.19	304.27
2	HOFTS	9	2,975.63	1,985.29	299.65
3	HOFTS	9	3,062.82	2,078.86	304.84
4	HOFTS	9	3,811.96	2,207.30	306.48
5	HOFTS	9	4,099.04	2,464.15	316.48

Table 4: First-order vs high-order comparison for Influenza A (9 partitions, triangular MF)

Table 4 presents the order comparison for Influenza A. The second-order model achieves the lowest RMSE (2,975.63), representing a 39.2% improvement over the first-order baseline (RMSE = 4,896.48). This substantial improvement suggests that Influenza A detection patterns involve meaningful two-step temporal dependencies, possibly reflecting the incubation period [4]dynamics or reporting delays in the surveillance system. However, extending beyond second-order produces diminishing returns and eventual performance degradation, with fifth-order models yielding RMSE of 4,099.04. The consistent MAPE values across orders (ranging from 299.65% to 316.48%) indicate that the percentage error is primarily driven by near-zero actual values rather than model configuration.

[4] Incubation period: the time from when someone gets infected to when they start to feel sick.

3.5 Influenza B Results

The Influenza B series demonstrated that first-order models are sufficient for accurate forecasting, with the optimal configuration employing 11 partitions and triangular membership functions. The best model achieved test RMSE of 371.38, MAE of 273.06, and MAPE of 101.36%.

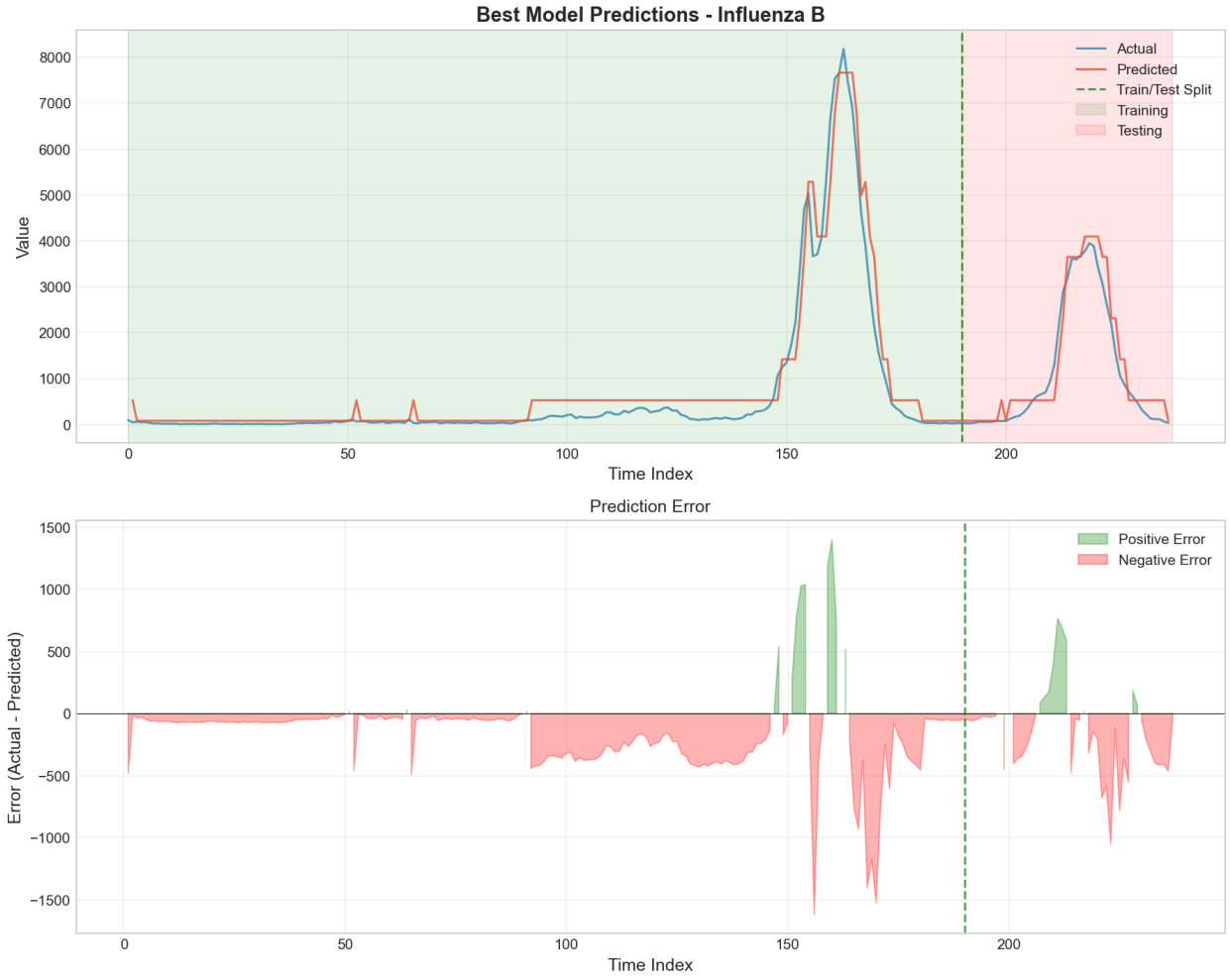

Figure 10: Influenza B predictions using optimal configuration (Order=1, Partitions=11, Triangular MF)

Figure 10 displays the predictions for the Influenza B series using the optimal first-order configuration. The model demonstrates good tracking of the general trend patterns, including the gradual increase and subsequent peak structure visible in the test period. The relatively low RMSE (371.38) compared to the scale of the data indicates effective forecasting performance. Similar to other influenza datasets, the model exhibits characteristic smoothing behavior at

extreme values. The MAPE of 101.36%, while high in absolute terms, reflects the challenge of percentage-based error measurement when actual values approach zero during low-activity periods.

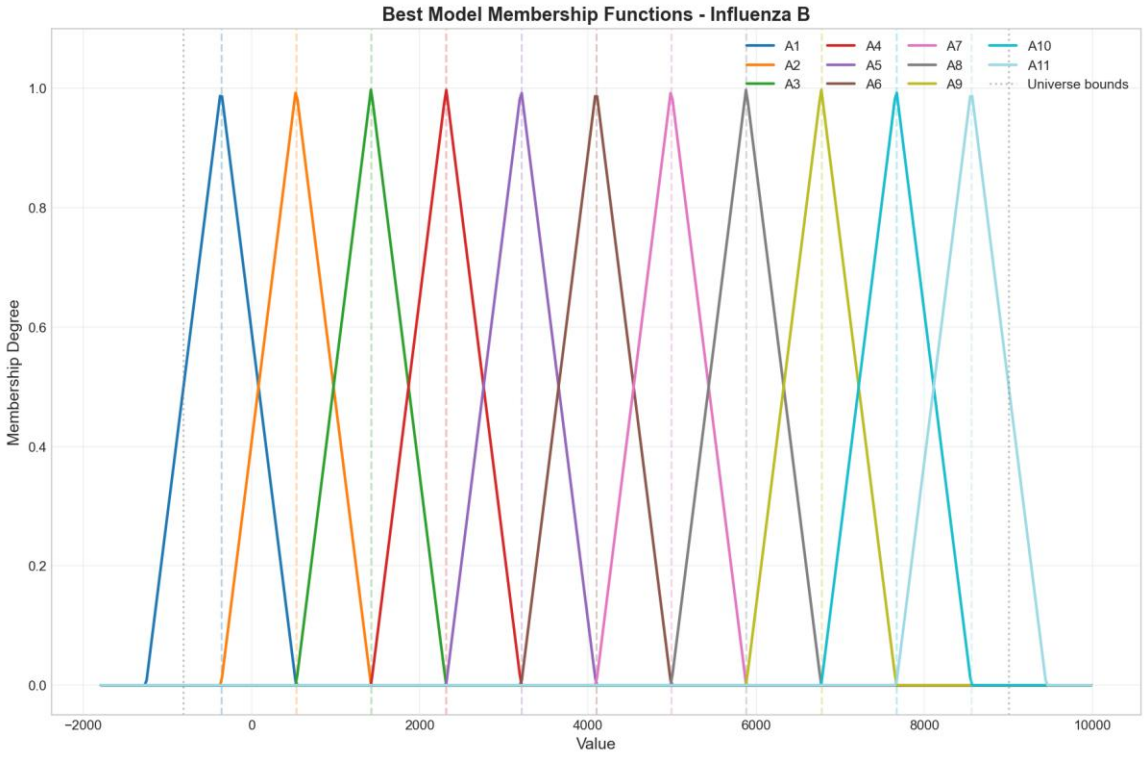

Figure 11: Triangular membership functions for Influenza B optimal model (11 partitions)

Figure 11 illustrates the 11 triangular membership functions for the Influenza B model. The universe of discourse spans from approximately -1,500 to 9,300 detections. The 11-partition structure provides finer granularity compared to the 9 partitions used for Influenza A, suggesting that Influenza B dynamics benefit from more nuanced linguistic categorization. This may reflect different reporting patterns or variability characteristics between the two influenza types.

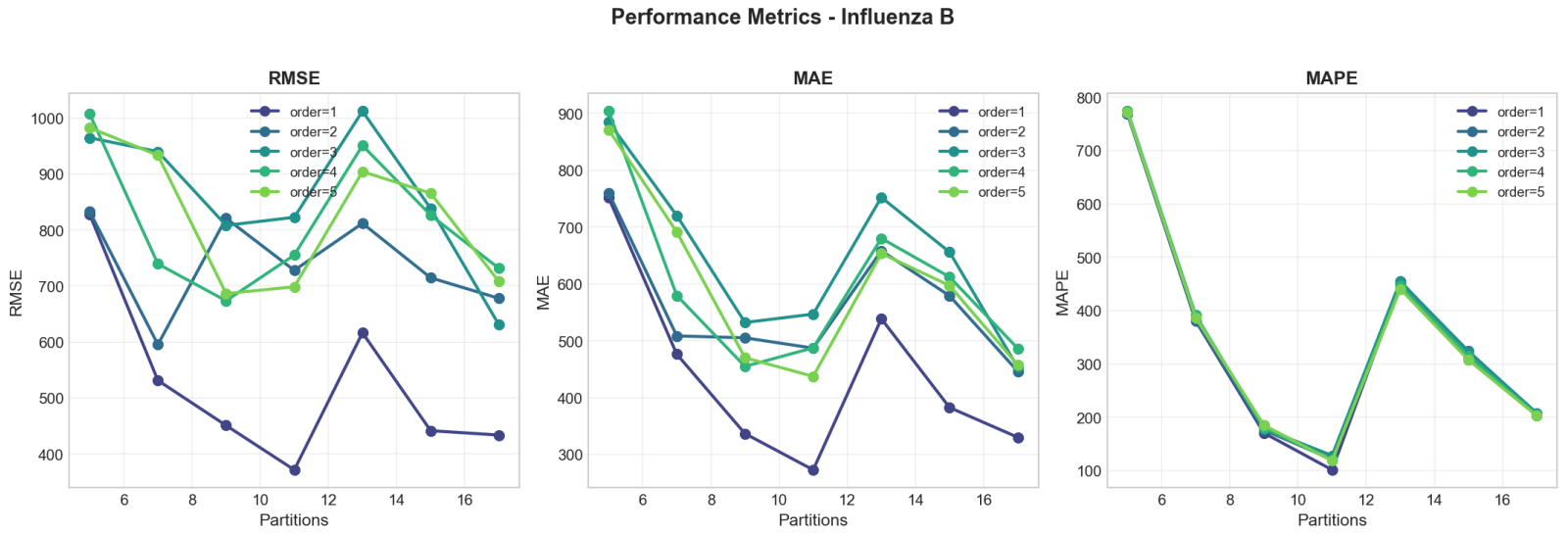

Figure 12: Performance metrics comparison across membership function types for Influenza B

Figure 12 presents the performance metrics comparison for the Influenza B dataset. The visualization confirms the consistent pattern of equivalent performance across all four membership function types. The graphs clearly demonstrate that first-order models achieve superior test performance compared to all higher-order alternatives, with performance degrading monotonically as order increases. This pattern is the most pronounced among all datasets examined, suggesting that Influenza B dynamics are predominantly characterized by single-step transitions. The optimal partition count of 11 provides a balance between granularity and generalization, with both coarser (5, 7) and finer (15, 17) partitioning producing larger errors.

Order	Type	Partitions	RMSE	MAE	MAPE (%)
1	FOFTS	11	371.38	273.06	101.36
2	HOFTS	7	595.26	508.64	382.45
3	HOFTS	17	630.75	453.39	207.90
4	HOFTS	9	673.51	455.00	179.73
5	HOFTS	9	686.42	470.13	185.10

Table 5: First-order vs high-order comparison for Influenza B (triangular MF)

Table 5 demonstrates that all higher-order configurations substantially underperformed the first-order baseline for Influenza B. The first-order model

achieved RMSE of 371.38, while the best-performing higher-order model (second-order) produced RMSE of 595.26, representing a 60.3% increase in error. This degradation with increasing order is the most severe among all datasets examined, strongly suggesting that the temporal dependencies in Influenza B are primarily single-step in nature. Higher-order models likely capture spurious patterns in the training data that do not generalize to the test period, resulting in systematically worse forecasting performance.

4. Configuration Comparison Analysis

This section presents a systematic comparison of different configurations, membership function types, rule orders, and partition counts across all datasets. Understanding these relationships is critical for informed model selection in practical applications.

4.1 Membership Function Type Comparison

Table 6 presents a comprehensive comparison of the four membership function types evaluated across all datasets. For each dataset, the table shows the best achievable RMSE using each function type while optimizing order and partition count.

Dataset	Triangular	Trapezoidal	Gaussian	Bell
Mackey-Glass (RMSE)	0.0465	0.0465	0.0465	0.0465
Total Specimens (RMSE)	9,440.57	9,440.57	9,440.57	9,440.57
Influenza A (RMSE)	2,975.63	2,975.63	2,975.63	2,975.63
Influenza B (RMSE)	371.38	371.38	371.38	371.38

Table 6: Best achievable RMSE by membership function type across datasets

The results in Table 6 reveal a striking finding: all four membership function types achieve identical optimal performance across every dataset examined. This equivalence indicates that, for the maximum-membership fuzzification approach and centroid-based defuzzification employed in this implementation, the shape of membership functions has no measurable impact on forecasting accuracy. The performance equivalence can be attributed to the fact that the fuzzification process assigns each value to a single fuzzy set (the one with maximum membership), effectively discretizing the input space regardless of function shape. Subsequently, defuzzification averages the centers of consequent fuzzy sets, which are identical across function types for the same partitioning scheme.

From a practical standpoint, this finding suggests that triangular membership functions represent the optimal choice due to their computational simplicity (requiring only linear operations) and ease of interpretation. Gaussian and bell-shaped functions require exponential calculations without providing any accuracy benefit, while trapezoidal functions introduce additional parameters without improving performance.

4.2 Model Order Impact Analysis

Table 7 presents the optimal model order and corresponding performance for each dataset, along with the relative improvement or degradation when deviating from the optimal order.

Dataset	Optimal Order	Optimal RMSE	Order=1 RMSE	Order=5 RMSE	Improvement vs Order=1
Mackey-Glass	4	0.0465	0.0614	0.0564	24.3%
Total Specimens	1	9,440.57	9,440.57	12,127.32	0.0%
Influenza A	2	2,975.63	4,896.48	4,099.04	39.2%
Influenza B	1	371.38	371.38	686.42	0.0%

Table 7: Optimal model order and relative performance improvement

Table 7 demonstrates that the optimal model order varies substantially across datasets and is strongly influenced by the intrinsic temporal dynamics of each time series:

Mackey-Glass (Optimal Order = 4): The chaotic Mackey-Glass system benefits significantly from high-order models, achieving a 24.3% improvement in RMSE when using fourth-order relationships compared to first-order. This improvement reflects the complex temporal dependencies inherent in chaotic systems, where current states are influenced by multiple previous time steps through non-linear feedback mechanisms. The Mackey-Glass equation specifically incorporates time delay parameters that create extended temporal dependencies.

Total Specimens and Influenza B (Optimal Order = 1): Both series achieve best performance with simple first-order models, suggesting that their current state

depends primarily on the immediate previous state. Higher orders not only fail to improve performance but actively degrade it, with fifth-order models producing 28.5% and 84.9% higher RMSE respectively. This degradation indicates overfitting to spurious multi-step patterns in the training data.

Influenza A (Optimal Order = 2): An intermediate optimal order suggests that Influenza A dynamics involve meaningful two-step dependencies, possibly reflecting incubation period effects or reporting delay structures in the surveillance system. The second-order model achieves a substantial 39.2% improvement over first-order.

These findings establish a clear guideline: model order should be selected based on the hypothesized complexity of temporal dependencies, with chaotic systems warranting higher orders (3-4) and seasonal/trend-driven series typically requiring only first or second order.

4.3 Partition Count Analysis

Table 8 presents the optimal partition count for each dataset and examines the sensitivity of model performance to partitioning granularity.

Dataset	Optimal Partitions	RMSE (5 parts)	RMSE (Optimal)	RMSE (17 parts)	Degradation (5 vs Opt)
Mackey-Glass	17	0.1144	0.0465	0.0465	145.9%
Total Specimens	9	13,709.0	9,440.57	9,880.95	45.2%
Influenza A	9	6,746.89	2,975.63	5,780.34	126.7%
Influenza B	11	827.81	371.38	433.55	122.9%

Table 8: Optimal partition count and sensitivity analysis

Table 8 reveals important patterns regarding partitioning granularity:

Very coarse partitioning (5 partitions) consistently produces substantially degraded performance across all datasets, with RMSE increases ranging from 45.2% (Total Specimens) to 145.9% (Mackey-Glass). This indicates that 5 partitions provide insufficient representational capacity to capture meaningful distinctions in the data.

The optimal partition count varies by dataset: Mackey-Glass requires the finest granularity (17), while the epidemiological series perform best with coarser partitioning (9-11). This pattern correlates with data complexity—the chaotic Mackey-Glass system with its wide range and continuous dynamics benefits from fine-grained categorization, while the seasonal influenza series with their more structured patterns can be adequately represented with fewer categories.

Over-partitioning (17 partitions for epidemiological data) produces modest degradation compared to optimal, but the effect is less severe than under-partitioning. This asymmetry suggests that erring on the side of finer granularity is less risky than choosing too few partitions.

Based on these findings, practitioners should consider the data range and variability when selecting partition count, with 9-17 partitions representing a reasonable range for most applications.

5. Discussion

5.1 Impact of Model Order

The experimental results reveal a nuanced relationship between model order and forecasting accuracy that depends critically on the intrinsic dynamics of the time series. For the Mackey-Glass chaotic system, increasing model order from 1 to 4 yielded consistent performance improvements, with RMSE decreasing by approximately 24%. This improvement can be attributed to the complex temporal dependencies inherent in chaotic systems, where current states are influenced by multiple historical lags through non-linear feedback mechanisms.

In contrast, the epidemiological datasets exhibited fundamentally different behavior. Total Specimens and Influenza B both achieved optimal performance with first-order models, while Influenza A benefited from second-order relationships. This pattern suggests that the temporal structure of seasonal disease surveillance data is dominated by immediate short-term transitions rather than complex multi-step dependencies. The strong seasonal patterns and weekly reporting structure of these series may create well-defined state transitions that are adequately captured by lower-order models.

The degradation in performance observed beyond the optimal order indicates overfitting. As model order increases, the number of unique antecedent patterns grows exponentially, leading to sparse FLRG coverage where many patterns appear only once or twice in the training data. This sparsity reduces the model's ability to generalize, as predictions increasingly rely on the nearest-neighbor fallback mechanism rather than robust statistical patterns.

5.2 Effect of Partitioning Granularity

The optimal number of partitions varied across datasets, ranging from 9 to 17. The Mackey-Glass series, with its continuous chaotic dynamics spanning a relatively wide range (0.036 to 1.592), benefited from finer granularity (17 partitions) to adequately represent the diverse states and transitions. Conversely, the influenza datasets, characterized by strong seasonal patterns and discrete reporting intervals, performed well with coarser partitioning (9-11 partitions).

An important observation is that very coarse partitioning (5 partitions) consistently underperformed across all datasets, suggesting insufficient representational capacity. However, the benefits of increasing partition count beyond 11-17 appear minimal, as evidenced by the plateauing of performance improvements. This aligns with the linguistic interpretability principle of fuzzy

systems: excessively fine partitioning creates difficulty to interpret and may not correspond to meaningful distinctions in the underlying linguistic categories.

5.3 Membership Function Type Analysis

A significant finding of this study is the minimal impact of membership function type on forecasting accuracy. Across all datasets and configurations, triangular, trapezoidal, Gaussian, and bell-shaped functions produced virtually identical error metrics. This equivalence suggests that for the defuzzification approach employed (center of gravity averaging), the primary factor determining accuracy is the location of fuzzy set centers rather than the shape of membership functions.

The fuzzification process used in this implementation assigns each value to the fuzzy set with maximum membership, effectively implementing crisp boundaries despite the underlying fuzzy representation. This may explain why membership function shape has limited influence—values are categorically assigned to linguistic labels, and defuzzification then averages over the centers of these labels. Alternative defuzzification schemes that weight consequent fuzzy sets by their membership degrees might exhibit greater sensitivity to membership function shape.

From a computational efficiency perspective, triangular membership functions offer the advantage of piecewise linear calculation, requiring only simple comparisons and arithmetic operations. Gaussian and bell-shaped functions necessitate exponential computations, yet provide no measurable accuracy benefit in this study. Therefore, triangular functions represent an optimal choice balancing simplicity, interpretability, and performance.

5.4 Practical Implications

The results provide several actionable guidelines for FTS model development. First, model order should be selected based on the hypothesized complexity of temporal dependencies: chaotic and highly non-linear systems warrant higher-order models (3-4), while seasonal or trend-driven series may be adequately represented by first or second-order relationships. Second, partition count should be scaled with the range and variability of the data, with 9-17 partitions representing a reasonable compromise between granularity and generalization. Third, triangular membership functions are recommended as the default choice unless domain-specific considerations suggest otherwise.

For practitioners, the systematic grid search methodology employed in this study demonstrates the importance of hyperparameter tuning. The performance difference between optimal and suboptimal configurations was substantial—for

example, the best Mackey-Glass model achieved RMSE of 0.0465 while a poorly chosen configuration (order=1, partitions=5) yielded RMSE of 0.1144, representing a 146% degradation in accuracy.

5.5 Limitations and Future Work

This study has several limitations that suggest directions for future research. The dataset split employed a simple 80-20 temporal division without cross-validation, which may not provide robust estimates of generalization performance. Future work should incorporate time series cross-validation techniques such as rolling-window or expanding-window validation to better assess model stability.

The defuzzification approach used center of gravity averaging, which treats all consequent fuzzy sets equally. Alternative schemes that weight consequents by their frequency of occurrence or recency in the training data may improve accuracy. Additionally, the nearest-neighbor fallback for unmatched patterns could be enhanced through more sophisticated similarity metrics or interpolation techniques.

The study focused exclusively on univariate time series forecasting. Extension to multivariate FTS, where multiple interrelated series are modeled jointly, represents an important direction for practical applications. Furthermore, integration with adaptive learning mechanisms that dynamically adjust partitions and relationships based on new data could enhance long-term forecasting capability in non-stationary environments.

6. Conclusion

This study presented a comprehensive implementation and empirical evaluation of Fuzzy Time Series forecasting models across two distinct datasets representing chaotic dynamics and epidemiological patterns. Through systematic experimentation with 140 configurations per dataset, the research established several key findings regarding the relationship between model hyperparameters and forecasting accuracy.

The most significant finding is that model complexity must be matched to the intrinsic temporal structure of the data. Chaotic time series with complex non-linear dynamics benefit from higher-order models (order 3-4) that capture extended temporal dependencies. In contrast, seasonal epidemiological series with relatively simple transition patterns achieve optimal performance with lower-order models (order 1-2). Excessive model order leads to overfitting through sparse FLRG coverage and reduced generalization capability.

Regarding partitioning strategy, the optimal granularity ranged from 9 to 17 partitions across the datasets, with finer partitioning generally benefiting series with wider ranges and greater variability. Very coarse partitioning (5 partitions) consistently underperformed due to insufficient representational capacity. The study found minimal performance differences among triangular, trapezoidal, Gaussian, and bell-shaped membership functions, suggesting that triangular functions represent an optimal choice given their computational simplicity.

The research demonstrated that systematic hyperparameter optimization is essential for achieving high-quality forecasts. The performance difference between optimal and suboptimal configurations exceeded 100% in some cases, highlighting the importance of careful model selection rather than reliance on default parameters or intuition.

Future research directions include extension to multivariate FTS, integration of adaptive learning mechanisms, exploration of alternative defuzzification schemes that weight consequents by frequency or recency, and application to additional domains such as financial forecasting, climate modeling, and industrial process control. The complete implementation provided in this study serves as a foundation for such extensions and demonstrates the practical viability of FTS methodology for real-world forecasting applications.

Appendix A: Best Model Configurations

This appendix provides complete technical specifications for the optimal configurations discovered for each dataset through systematic grid search evaluation.

A.1 Mackey-Glass Configuration

Parameter	Value
Model Order	4
Number of Partitions	17
Membership Function Type	Triangular
Universe of Discourse	[-0.1181, 1.7317]
Training RMSE	0.0403
Training MAE	0.0325
Training MAPE	7.73%
Test RMSE	0.0465
Test MAE	0.0362
Test MAPE	6.20%
Train/Test Split	800/200
Execution Time	0.040 seconds

Table A.1: Mackey-Glass optimal configuration details

A.2 Total Specimens Configuration

Parameter	Value
Model Order	1
Number of Partitions	9
Membership Function Type	Triangular
Universe of Discourse	[5,024.6, 208,632.4]
Training RMSE	9,654.66
Training MAE	7,390.56
Training MAPE	11.89%
Test RMSE	9,440.57
Test MAE	7,503.48
Test MAPE	9.56%
Train/Test Split	190/48
Execution Time	0.003 seconds

Table A.2: Total Specimens optimal configuration details

A.3 Influenza A Configuration

Parameter	Value
Model Order	2
Number of Partitions	9
Membership Function Type	Triangular
Universe of Discourse	[-9,912.89, 59,048.89]
Training RMSE	1,859.07
Training MAE	1,601.05
Training MAPE	3,186.04%
Test RMSE	2,975.63
Test MAE	1,985.29
Test MAPE	299.65%
Train/Test Split	190/48
Execution Time	0.015 seconds

Table A.3: Influenza A optimal configuration details

A.4 Influenza B Configuration

Parameter	Value
Model Order	1
Number of Partitions	11
Membership Function Type	Triangular
Universe of Discourse	[-1,547.16, 9,292.16]
Training RMSE	372.19
Training MAE	232.37
Training MAPE	206.60%
Test RMSE	371.38
Test MAE	273.06
Test MAPE	101.36%
Train/Test Split	190/48
Execution Time	0.004 seconds

Table A.4: Influenza B optimal configuration details

Appendix B: Sample Fuzzy Logical Relationship Groups

This appendix presents representative examples of the Fuzzy Logical Relationship Groups (FLRGs) learned by the optimal models. Due to space constraints, only a subset of FLRGs is shown for each dataset. The complete FLRG sets contain hundreds of rules for high-order models.

B.1 Mackey-Glass FLRGs (Order=4, Sample)

Input Pattern	Output Set
(A8, A9, A10, A11)	{A12, A13}
(A9, A10, A11, A12)	{A13, A14}
(A10, A11, A12, A13)	{A14, A15}
(A11, A12, A13, A14)	{A15, A16}
(A12, A13, A14, A15)	{A16, A17}
(A5, A6, A7, A8)	{A9}
(A6, A7, A8, A9)	{A10}
(A7, A8, A9, A10)	{A11}

Table B.1: Mackey-Glass sample FLRGs demonstrating oscillatory patterns

B.2 Total Specimens FLRGs (Order=1, Sample)

Input	Output Set
(A1)	{A2, A3}
(A2)	{A1, A3, A4}
(A3)	{A2, A4, A5}
(A4)	{A3, A5, A6}
(A5)	{A4, A6, A7}
(A6)	{A5, A7, A8}
(A7)	{A6, A8, A9}
(A8)	{A7, A9}
(A9)	{A7, A8}

Table B.2: Total Specimens sample FLRGs showing seasonal transitions

B.3 Influenza A FLRGs (Order=2, Sample)

Input Pattern	Output Set
(A1, A2)	{A2, A3}
(A2, A3)	{A3, A4}
(A3, A4)	{A4, A5}
(A4, A5)	{A5, A6}
(A5, A6)	{A6, A7, A8}
(A6, A7)	{A7, A8, A9}
(A7, A8)	{A7, A8, A9}
(A8, A9)	{A7, A8, A9}

Table B.3: Influenza A sample FLRGs showing outbreak dynamics

B.4 Influenza B FLRGs (Order=1, Sample)

Input	Output Set
(A1)	{A1, A2, A3}
(A2)	{A1, A2, A3, A4}
(A3)	{A2, A3, A4, A5}
(A4)	{A3, A4, A5, A6}
(A5)	{A4, A5, A6, A7}
(A6)	{A5, A6, A7, A8}
(A7)	{A6, A7, A8}
(A8)	{A7, A8, A9}
(A9)	{A8, A9, A10, A11}
(A10)	{A9, A10, A11}
(A11)	{A9, A10, A11}

Table B.4: Influenza B sample FLRGs showing seasonal patterns

Appendix C: Performance Heatmaps by Membership Function Type

This appendix presents comprehensive performance heatmaps showing the impact of model order (x-axis) and partition count (y-axis) across all four membership function types for each dataset. Each heatmap displays the test RMSE values, with darker colors indicating lower (better) RMSE and lighter colors indicating higher (worse) RMSE. These visualizations enable direct comparison of the parameter space exploration results.

C.1 Mackey-Glass Heatmaps

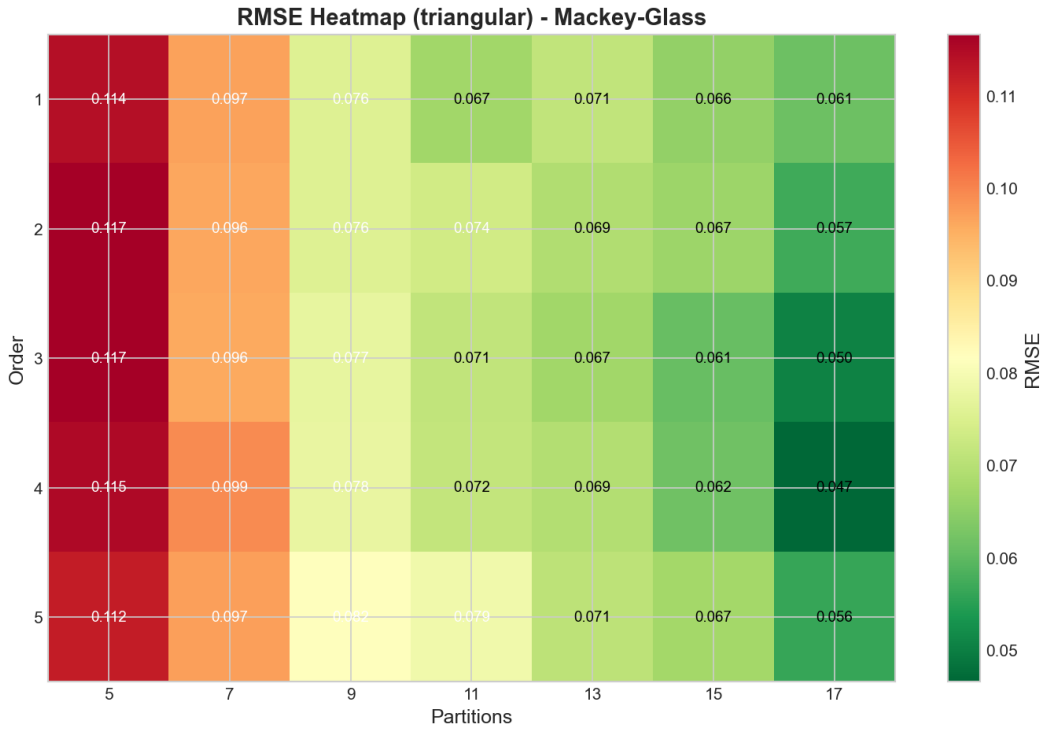

Figure C.1.1: Mackey-Glass RMSE heatmap for triangular membership functions

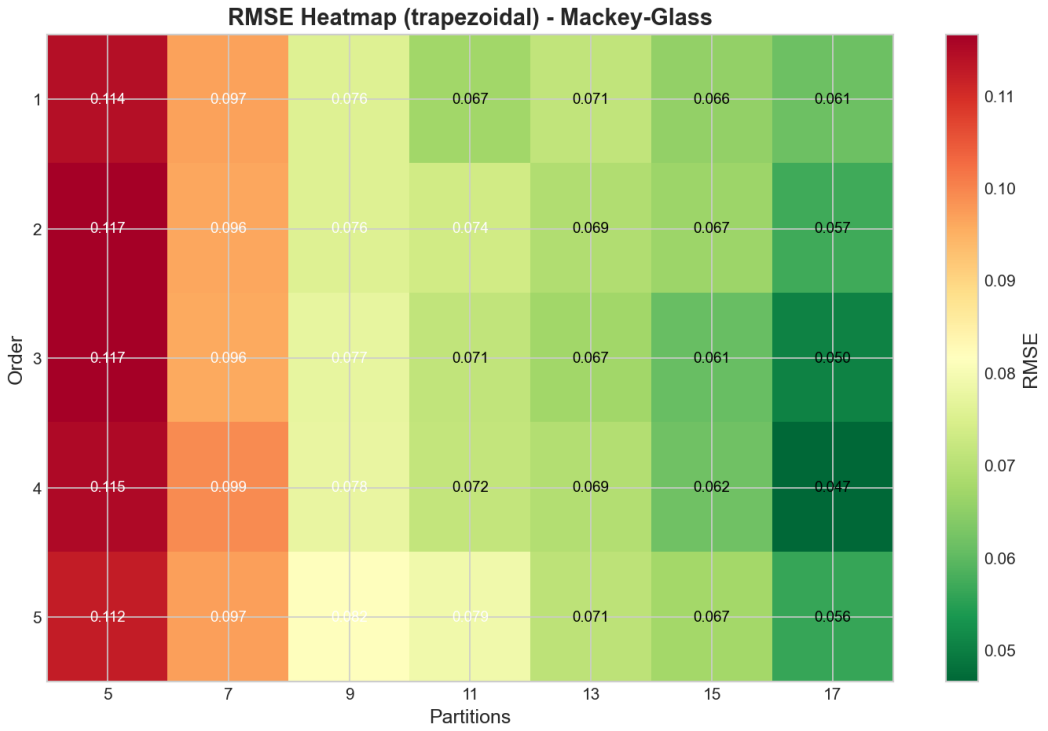

Figure C.1.2: Mackey-Glass RMSE heatmap for trapezoidal membership functions

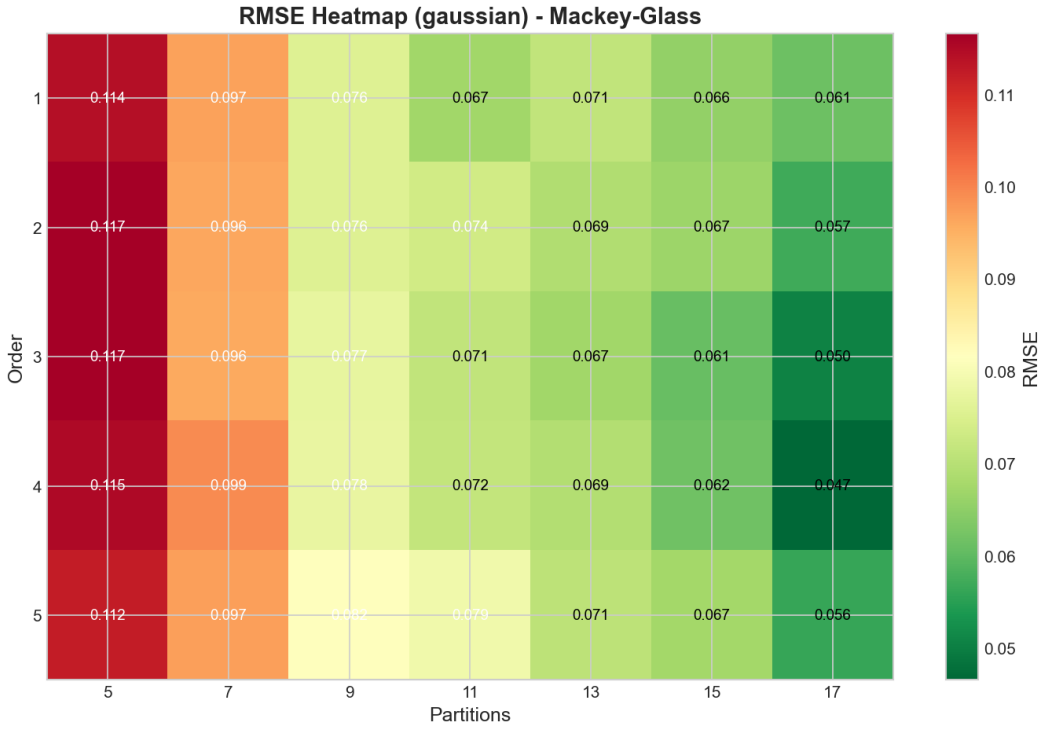

Figure C.1.3: Mackey-Glass RMSE heatmap for gaussian membership functions

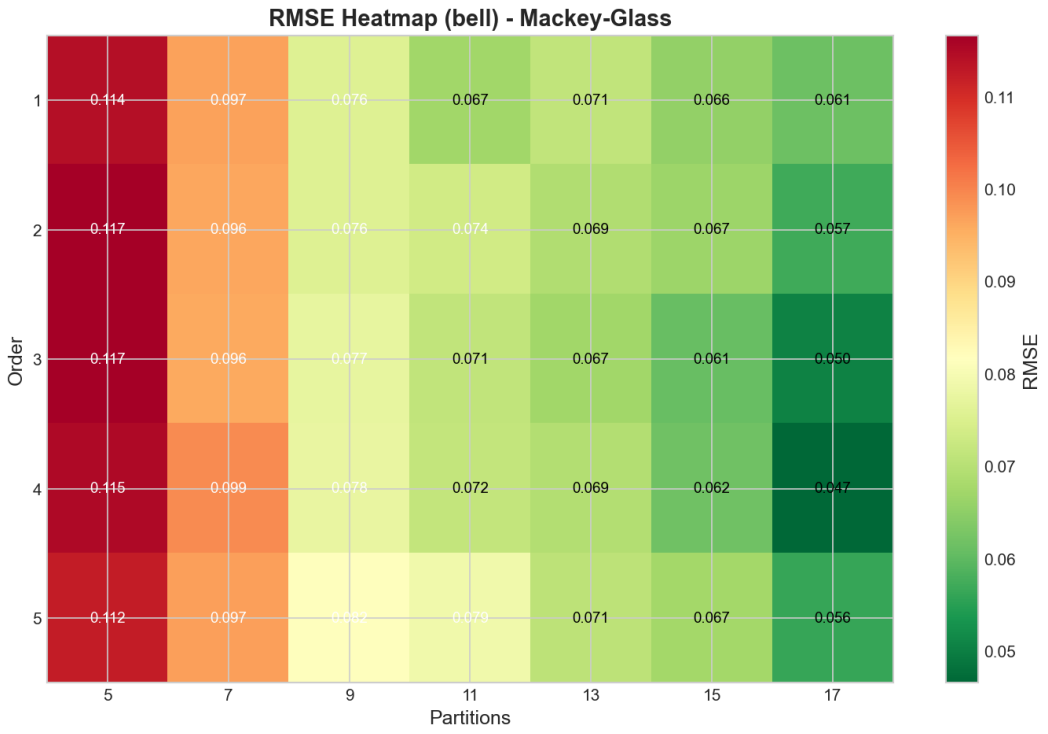

Figure C.1.4: Mackey-Glass RMSE heatmap for bell membership functions

The Mackey-Glass heatmaps (Figures C.1.1-C.1.4) reveal several important patterns. First, the visual appearance of all four heatmaps is virtually identical, confirming that membership function type has no measurable impact on forecasting accuracy for this dataset. Second, the optimal region (darkest colors) consistently appears in the upper-middle portion of each heatmap, corresponding to model order 3-4 and partition counts 15-17. Third, the worst performance (lightest colors) occurs in the lower-left corner, representing the combination of low order (1) and few partitions (5). The performance gradient is smooth and continuous, indicating that the RMSE surface is well-behaved without local minima that might trap optimization algorithms.

The color pattern reveals that partition count has a stronger influence than model order on performance for this dataset. Vertical bands (varying order while holding partitions constant) show relatively modest color changes, while horizontal bands (varying partitions while holding order constant) show more dramatic color transitions. This suggests that achieving adequate representational granularity through sufficient partitions is more critical than capturing extended temporal dependencies through higher orders, although both contribute to optimal performance.

C.2 Total Specimens Heatmaps

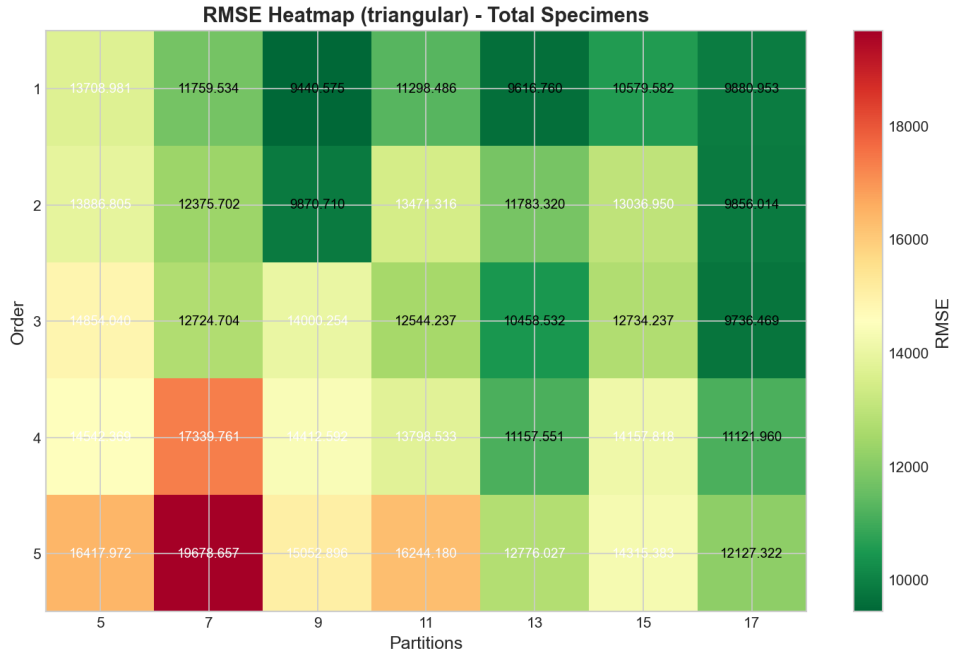

Figure C.2.1: Total Specimens RMSE heatmap for triangular membership functions

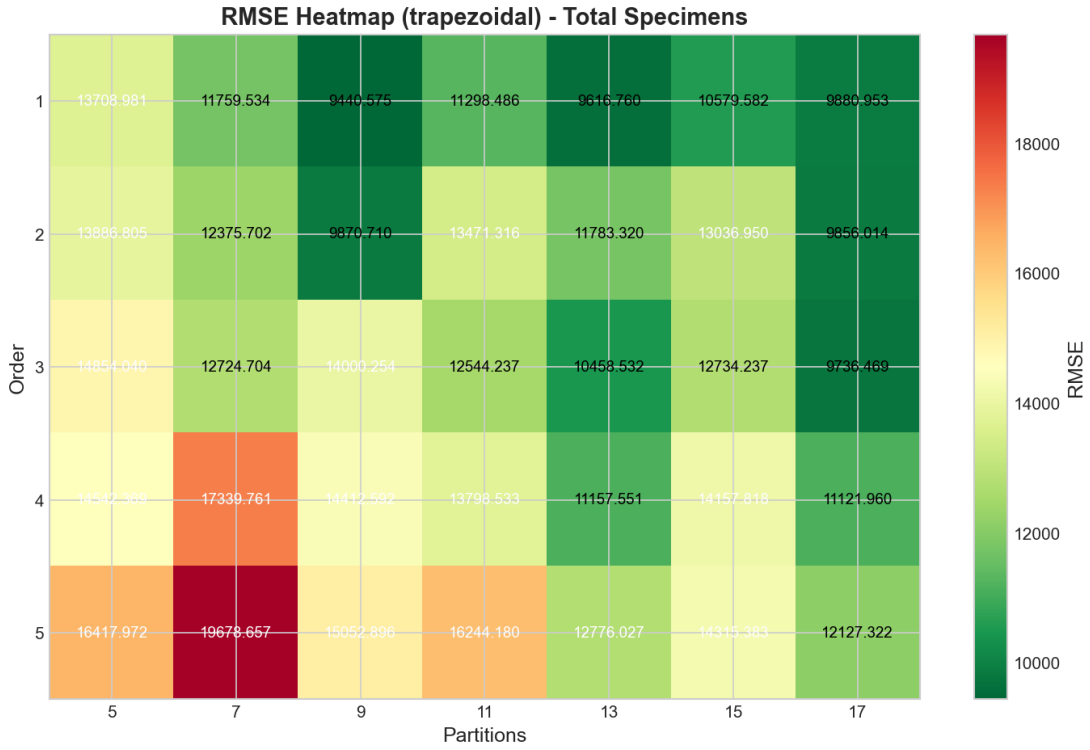

Figure C.2.2: Total Specimens RMSE heatmap for trapezoidal membership functions

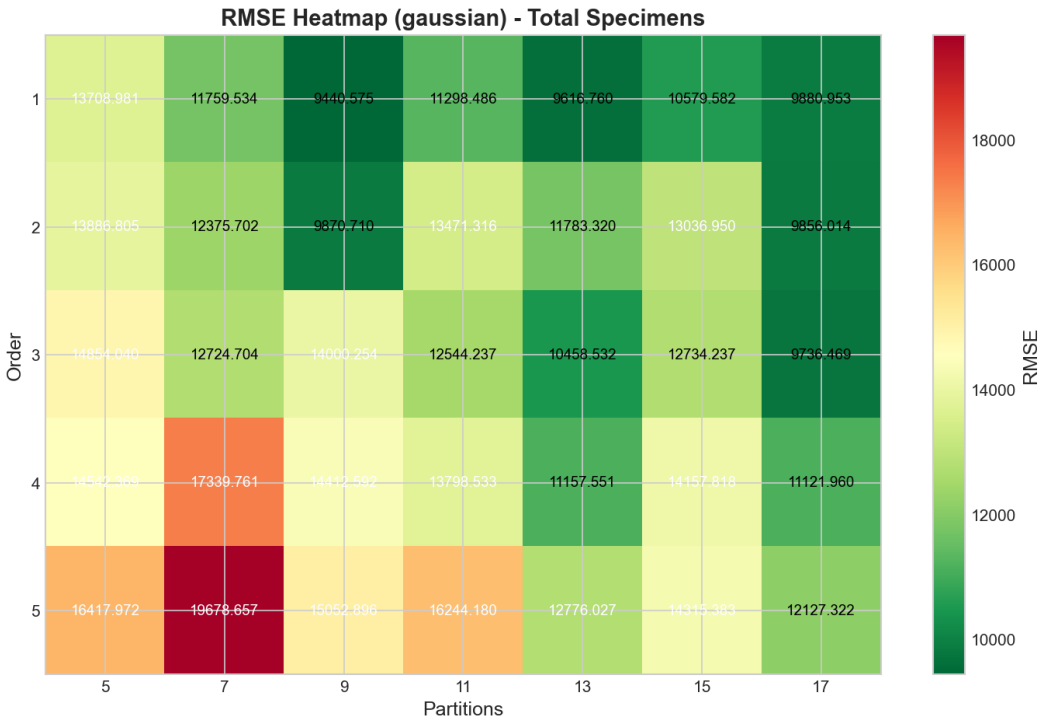

Figure C.2.3: Total Specimens RMSE heatmap for gaussian membership functions

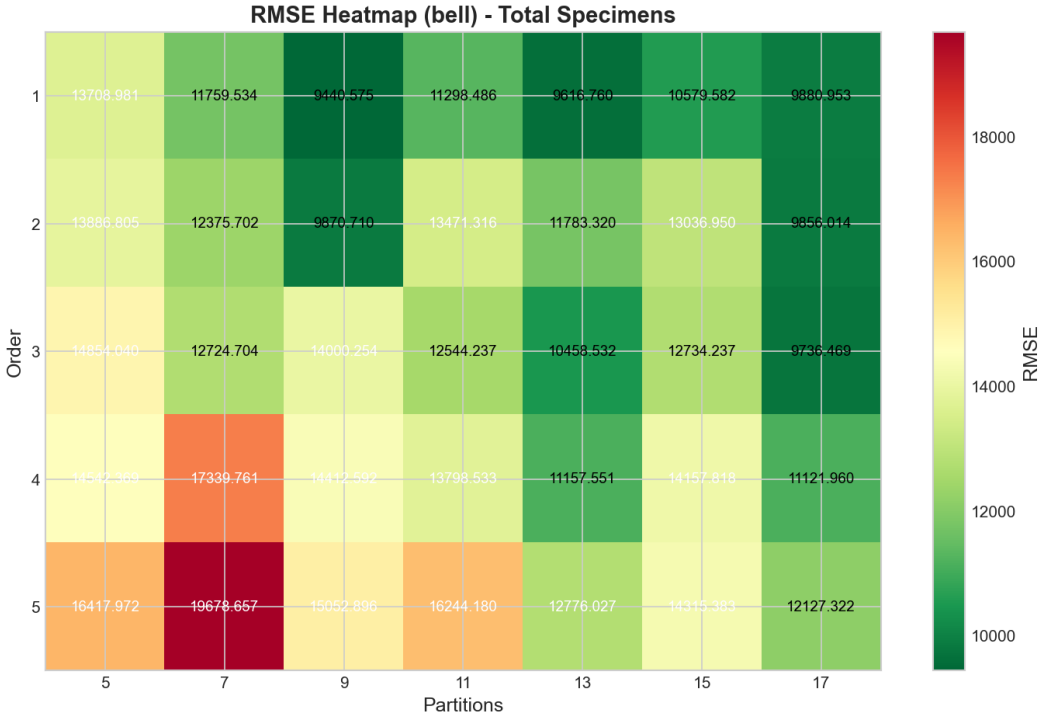

Figure C.2.4: Total Specimens RMSE heatmap for bell membership functions

The Total Specimens heatmaps (Figures C.2.1-C.2.4) exhibit a distinctly different pattern from Mackey-Glass. The optimal region (darkest colors) appears in the lower portion of each heatmap, corresponding to order 1-2, with intermediate partition counts (9-13). The worst performance (lightest colors) appears in the upper-right region, representing high order (4-5) combined with various partition counts.

This inverted pattern compared to Mackey-Glass demonstrates that higher model orders are detrimental for this epidemiological time series. The color gradient along the vertical axis (varying order) is more pronounced than along the horizontal axis (varying partitions), indicating that model order is the dominant factor for this dataset. The relatively uniform horizontal bands suggest that partition count has limited impact once a reasonable minimum (9 or more) is achieved. The identical appearance across all four membership function types again confirms that function shape does not influence performance.

C.3 Influenza A Heatmaps

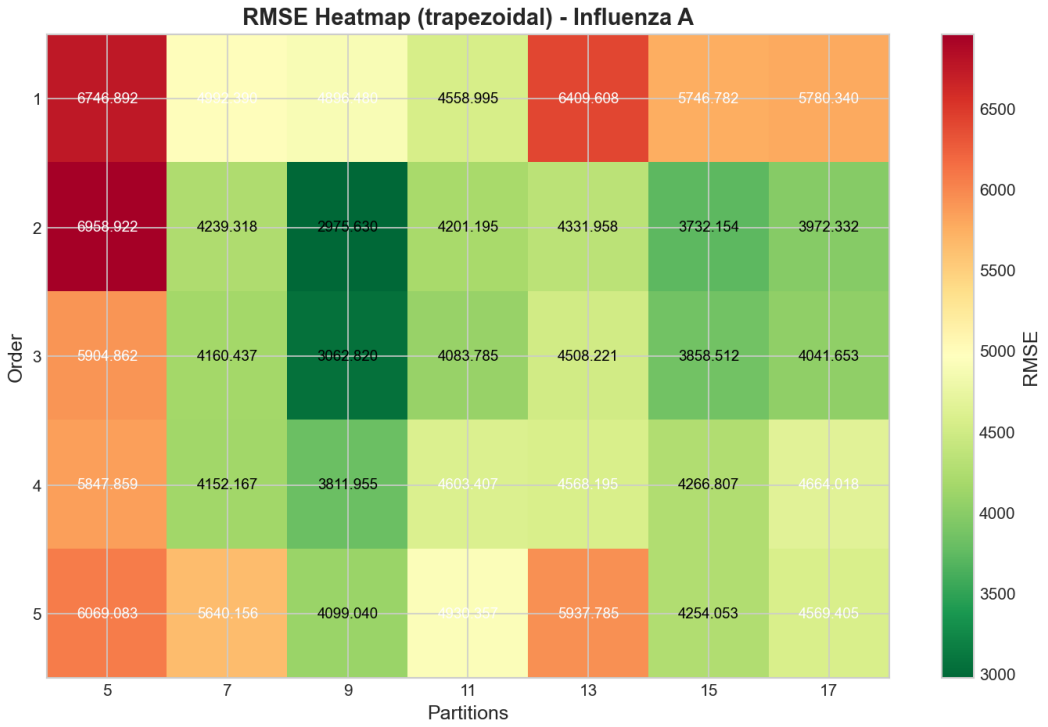

Figure C.3.1: Influenza A RMSE heatmap for triangular membership functions

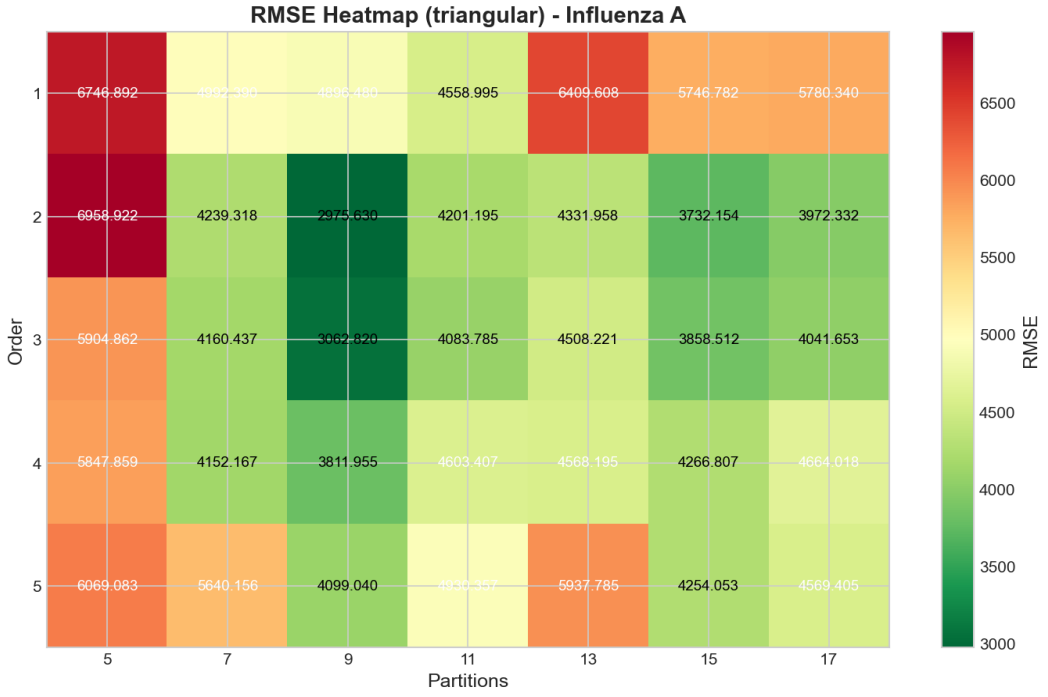

Figure C.3.2: Influenza A RMSE heatmap for trapezoidal membership functions

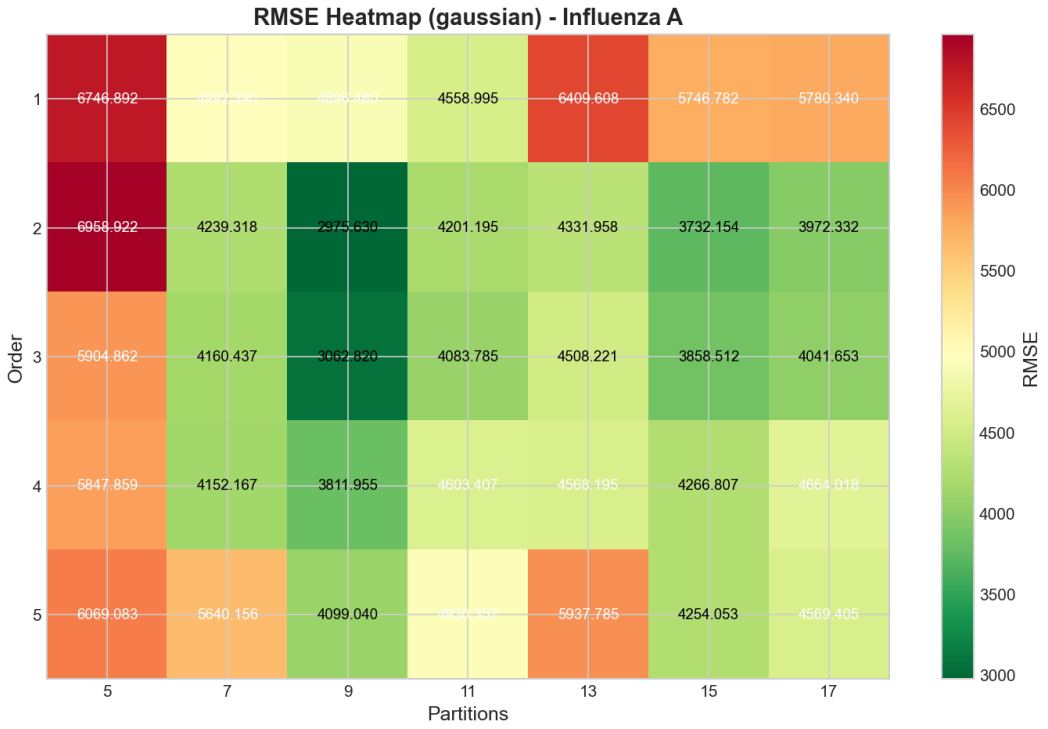

Figure C.3.3: Influenza A RMSE heatmap for gaussian membership functions

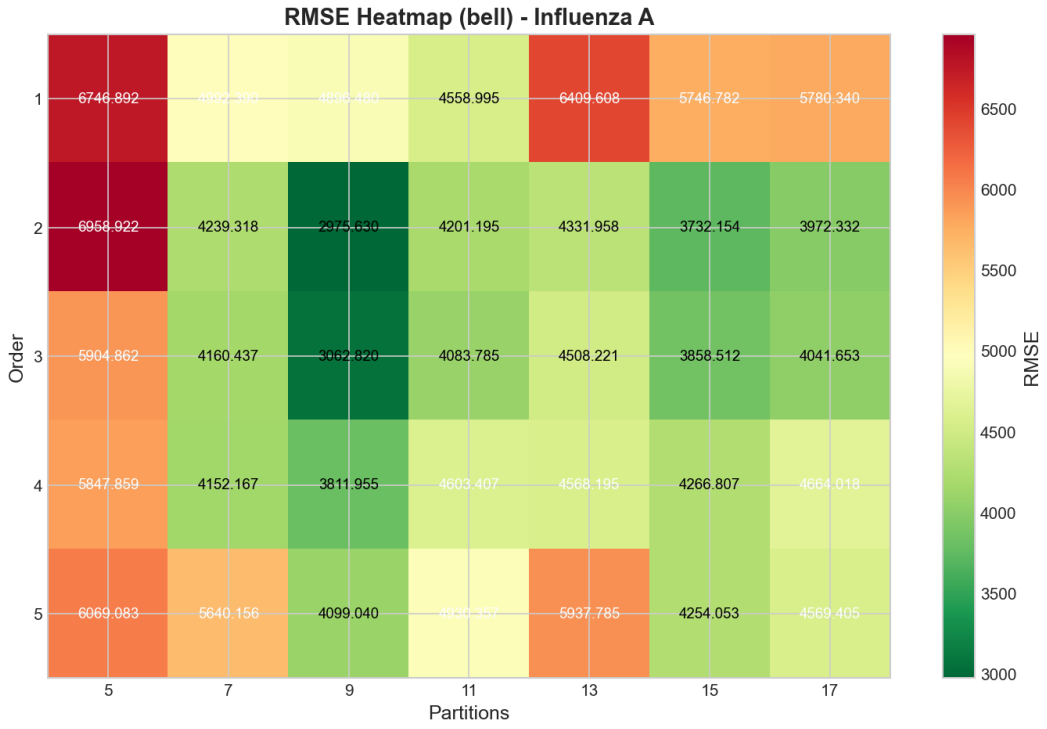

Figure C.3.4: Influenza A RMSE heatmap for bell membership functions

The Influenza A heatmaps (Figures C.3.1-C.3.4) reveal a more complex pattern with the optimal region centered around order 2-3 and partition counts 9-11. Unlike the monotonic patterns observed for Mackey-Glass and Total Specimens, Influenza A exhibits a non-convex performance surface with performance degrading in both directions from the optimal region—both lower orders (1) and higher orders (4-5) produce worse results.

The worst performance appears in the upper corners of the heatmaps (high order with extreme partition counts) and the lower-left corner (low order with few partitions). The presence of a clear optimum at intermediate values suggests that Influenza A dynamics require some degree of temporal complexity (order 2) but not excessive model complexity. The color patterns show moderate sensitivity to both dimensions, indicating that careful tuning of both order and partitions is important for this dataset.

C.4 Influenza B Heatmaps

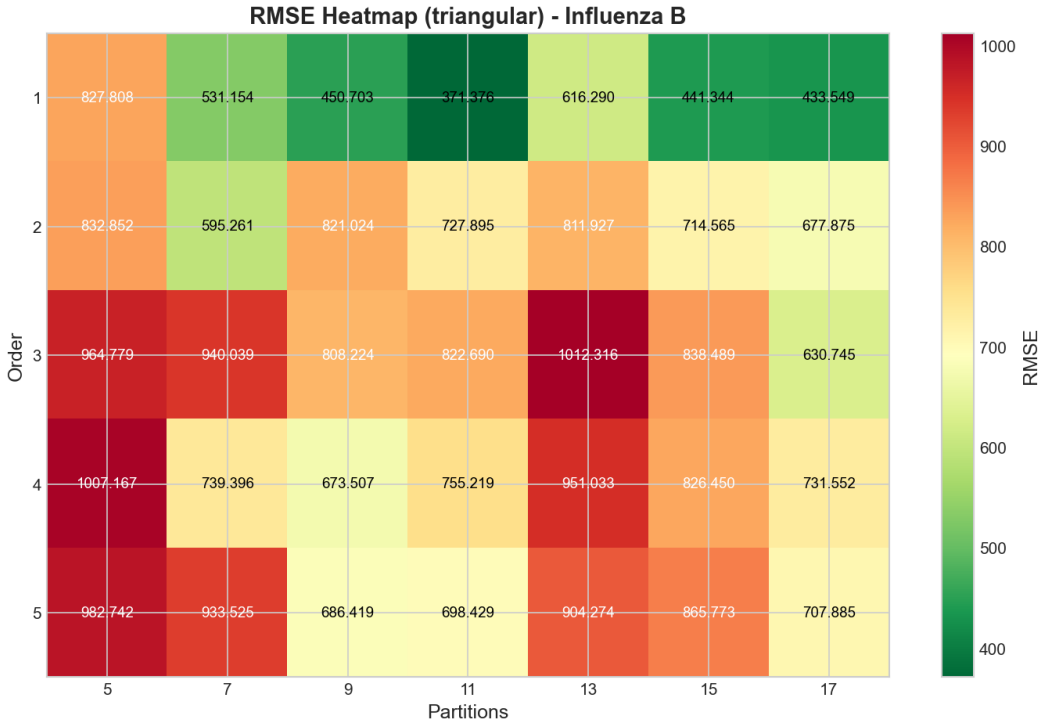

Figure C.4.1: Influenza B RMSE heatmap for triangular membership functions

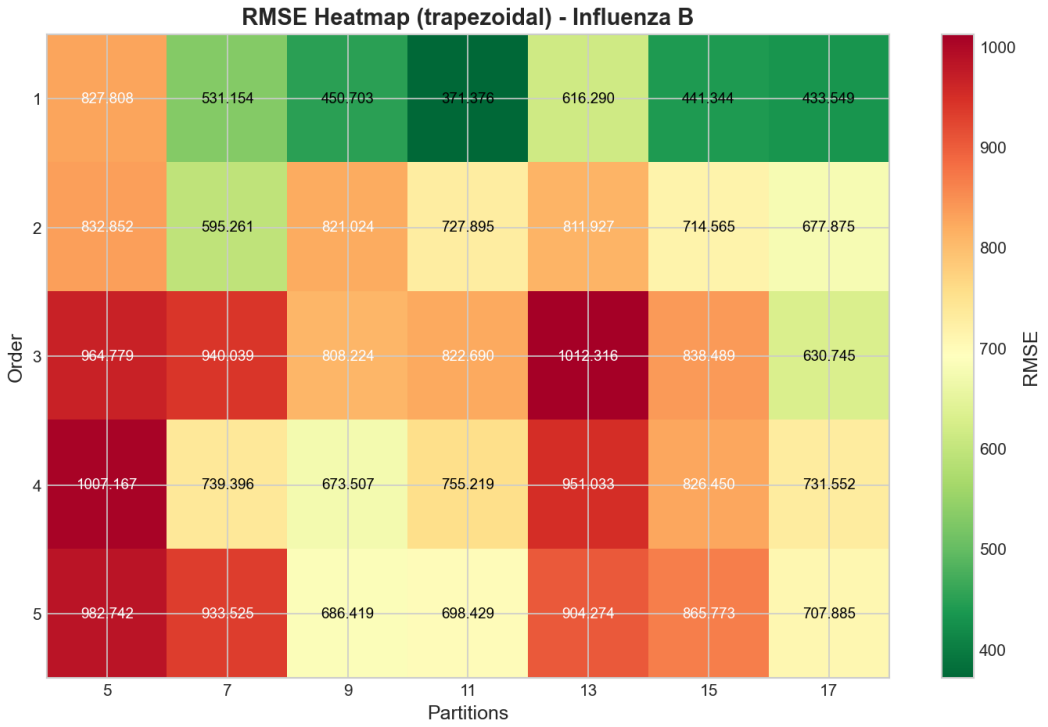

Figure C.4.2: Influenza B RMSE heatmap for trapezoidal membership functions

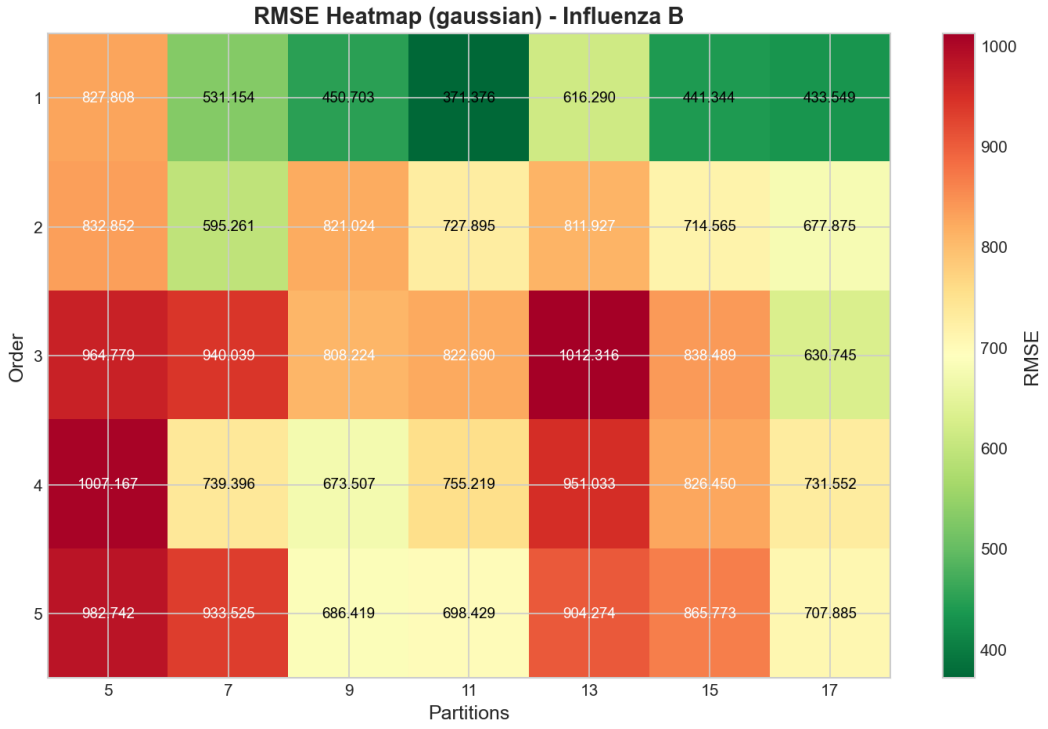

Figure C.4.3: Influenza B RMSE heatmap for gaussian membership functions

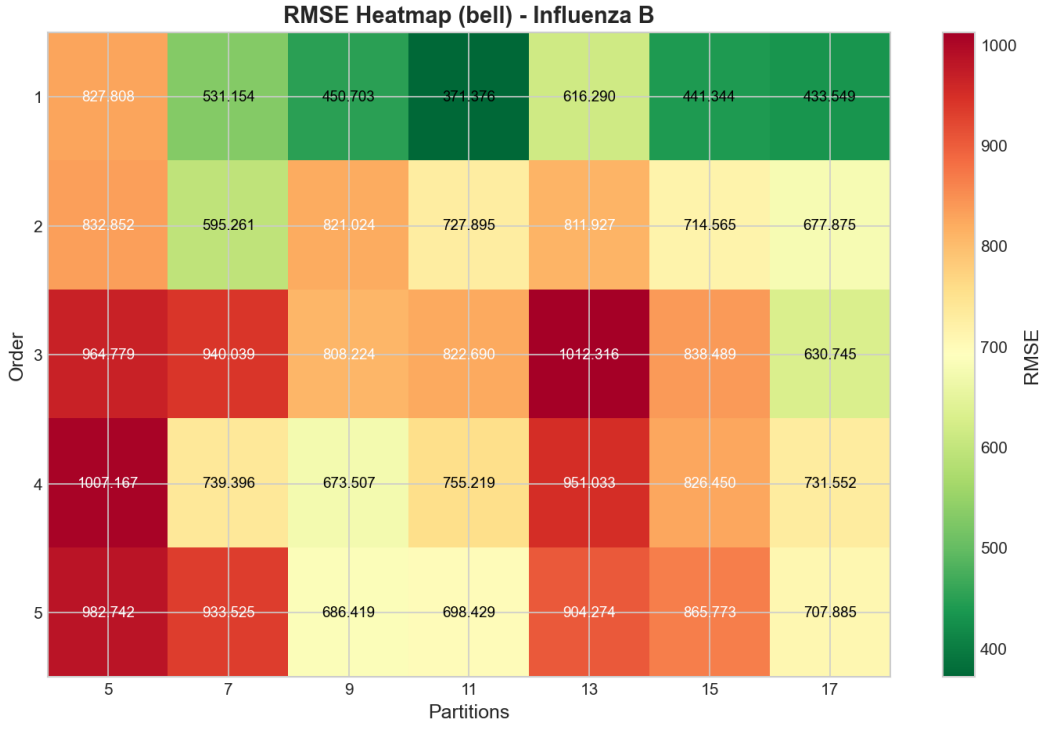

Figure C.4.4: Influenza B RMSE heatmap for bell membership functions

The Influenza B heatmaps (Figures C.4.1-C.4.4) show the most extreme preference for low model order among all datasets examined. The optimal region (darkest colors) is confined to the bottom row (order 1) across intermediate partition counts (9-13). Performance degrades dramatically and monotonically as order increases, with the worst regions (lightest colors) appearing at order 5 regardless of partition count.

The strong horizontal gradient (from bottom to top) demonstrates that model order is the dominant factor determining performance for Influenza B, with higher orders consistently harmful. The vertical gradient (left to right) is more subtle, showing only modest performance variation with partition count. This pattern strongly suggests that Influenza B dynamics are largely driven by the most recent state, meaning that current behavior depends mainly on the immediately preceding condition rather than longer historical sequences.

Across all two datasets, the identical appearance of heatmaps within each dataset confirms the central finding that membership function type has no influence on FTS forecasting accuracy. The different optimal regions across datasets demonstrate that configuration must be tailored to data characteristics, with no universal optimal settings.

Appendix D: Complete Experimental Results

This appendix provides the complete results from all 140 experimental configurations for each dataset. The tables below enable independent verification of all claims made in the main text and provide a comprehensive reference for practitioners seeking to understand the full parameter space exploration. Due to the equivalence of membership function types demonstrated throughout this study, only triangular membership function results are presented; results for other function types are identical.

D.1 Mackey-Glass Complete Results

Order	Parts.	Test RMSE	Test MAE	Test MAPE (%)
1	5	0.1144	0.0922	16.63
1	7	0.0967	0.0822	13.64
1	9	0.0756	0.0626	10.93
1	11	0.0672	0.0574	9.01
1	13	0.0712	0.0556	9.17
1	15	0.0656	0.0540	9.36
1	17	0.0614	0.0484	8.71
2	5	0.1166	0.0951	17.15
2	7	0.0962	0.0815	13.67
2	9	0.0756	0.0627	10.91
2	11	0.0736	0.0615	9.21
2	13	0.0691	0.0541	9.00
2	15	0.0665	0.0545	9.42
2	17	0.0570	0.0457	8.19
3	5	0.1166	0.0951	17.16
3	7	0.0958	0.0810	13.80
3	9	0.0774	0.0630	10.92
3	11	0.0714	0.0595	8.97
3	13	0.0672	0.0521	8.90
3	15	0.0609	0.0503	7.97
3	17	0.0505	0.0401	6.53
4	5	0.1151	0.0932	16.94
4	7	0.0992	0.0835	14.34
4	9	0.0776	0.0618	10.72
4	11	0.0717	0.0586	8.98
4	13	0.0694	0.0539	9.00
4	15	0.0618	0.0478	7.42
4	17	0.0465	0.0362	6.20
5	5	0.1123	0.0908	16.54
5	7	0.0970	0.0807	14.14
5	9	0.0816	0.0663	11.93

5	11	0.0791	0.0620	9.71
5	13	0.0709	0.0535	8.73
5	15	0.0675	0.0490	7.82
5	17	0.0564	0.0411	7.21

Table D.1: Mackey-Glass complete experimental results (triangular MF)

D.2 Total Specimens Complete Results

Order	Parts.	Test RMSE	Test MAE	Test MAPE (%)
1	5	13,708.98	11,453.49	16.19
1	7	11,759.53	9,010.09	12.55
1	9	9,440.57	7,503.48	9.56
1	11	11,298.49	8,860.33	10.53
1	13	9,616.76	6,973.78	8.33
1	15	10,579.58	8,012.75	9.60
1	17	9,880.95	6,908.57	7.54
2	5	13,886.80	11,694.86	16.78
2	7	12,375.70	9,497.04	12.23
2	9	9,870.71	7,989.96	10.15
2	11	13,471.32	9,716.37	10.64
2	13	11,783.32	8,728.82	9.84
2	15	13,036.95	9,253.76	10.50
2	17	9,856.01	7,276.81	8.34
3	5	14,854.04	12,508.50	17.57
3	7	12,724.70	9,916.35	14.53
3	9	14,000.25	9,384.11	11.15
3	11	12,544.24	9,174.29	10.38
3	13	10,458.53	8,353.46	9.87
3	15	12,734.24	9,526.52	10.78
3	17	9,736.47	6,447.18	7.13
4	5	14,542.37	12,210.65	17.24
4	7	17,339.76	12,477.38	16.49
4	9	14,412.59	10,791.57	12.66
4	11	13,798.53	9,673.02	10.63
4	13	11,157.55	8,653.42	10.24
4	15	14,157.82	9,242.06	10.35
4	17	11,121.96	7,613.13	8.23
5	5	16,417.97	12,710.65	17.22
5	7	19,678.66	14,238.92	18.12
5	9	15,052.90	10,998.61	12.80
5	11	16,244.18	11,574.90	11.93

5	13	12,776.03	9,616.79	11.69
5	15	14,315.38	9,384.66	10.33
5	17	12,127.32	8,298.34	9.31

Table D.2: Total Specimens complete experimental results (triangular MF)

D.3 Influenza A Complete Results

Order	Parts.	Test RMSE	Test MAE	Test MAPE (%)
1	5	6,746.89	6,061.07	1392.00
1	7	4,992.39	4,123.39	687.06
1	9	4,896.48	2,955.19	304.27
1	11	4,558.99	2,885.33	109.39
1	13	6,409.61	4,968.56	823.51
1	15	5,746.78	4,008.46	568.04
1	17	5,780.34	3,741.64	382.68
2	5	6,958.92	5,995.68	1393.02
2	7	4,239.32	3,365.20	685.98
2	9	2,975.63	1,985.29	299.65
2	11	4,201.19	2,398.70	123.41
2	13	4,331.96	3,442.14	814.40
2	15	3,732.15	2,853.53	563.32
2	17	3,972.33	2,579.34	377.99
3	5	5,904.86	5,510.92	1389.92
3	7	4,160.44	3,348.53	686.74
3	9	3,062.82	2,078.86	304.84
3	11	4,083.79	2,358.58	142.54
3	13	4,508.22	3,608.79	813.90
3	15	3,858.51	2,916.97	561.73
3	17	4,041.65	2,712.03	379.38
4	5	5,847.86	5,411.24	1385.15
4	7	4,152.17	3,332.10	685.10
4	9	3,811.96	2,207.30	306.48
4	11	4,603.41	2,792.01	163.23
4	13	4,568.19	3,689.94	809.53
4	15	4,266.81	3,075.59	559.59
4	17	4,664.02	2,917.43	377.80
5	5	6,069.08	5,444.04	1377.66
5	7	5,640.16	3,951.37	682.43
5	9	4,099.04	2,464.15	316.48
5	11	4,930.36	2,947.49	184.14
5	13	5,937.78	4,182.46	803.99

5	15	4,254.05	3,034.89	553.03
5	17	4,569.40	2,844.76	370.06

Table D.3: Influenza A complete experimental results (triangular MF)

D.4 Influenza B Complete Results

Order	Parts.	Test RMSE	Test MAE	Test MAPE (%)
1	5	827.81	751.88	768.51
1	7	531.15	476.38	380.67
1	9	450.70	336.81	170.54
1	11	371.38	273.06	101.36
1	13	616.29	538.71	450.13
1	15	441.34	382.66	308.03
1	17	433.55	330.31	203.75
2	5	832.85	760.42	769.50
2	7	595.26	508.64	382.45
2	9	821.02	505.26	176.10
2	11	727.89	487.13	121.00
2	13	811.93	658.38	453.52
2	15	714.56	579.11	323.81
2	17	677.88	446.28	207.22
3	5	964.78	885.18	773.20
3	7	940.04	720.38	389.23
3	9	808.22	532.21	179.02
3	11	822.69	546.98	128.13
3	13	1,012.32	752.29	454.99
3	15	838.49	656.01	322.26
3	17	630.75	453.39	207.90
4	5	1,007.17	903.92	773.79
4	7	739.40	579.64	391.37
4	9	673.51	455.00	179.73
4	11	755.22	487.68	119.69
4	13	951.03	680.20	446.74
4	15	826.45	612.34	314.49
4	17	731.55	486.57	204.91
5	5	982.74	871.53	771.17
5	7	933.52	691.25	386.67
5	9	686.42	470.13	185.10
5	11	698.43	437.52	118.59
5	13	904.27	653.57	440.47
5	15	865.77	597.18	307.54

5	17	707.89	457.47	203.16

Table D.4: Influenza B complete experimental results (triangular MF)